

Luminescent Platinum(II) Complexes with Bidentate Diacetylide Ligands: Structures, Photophysical Properties and Application Studies

Zaoli Luo,^[a] Yungen Liu,^[b] Ka-Chung Tong,^[c] Xiao-Yong Chang,^[b] Wai-Pong To,^{*,[c]} and Chi-Ming Che^{*,[b, c, d]}

Abstract: A series of platinum(II) complexes supported by terphenyl diacetylide as well as diimine or bis-*N*-heterocyclic carbene (NHC) ligands have been prepared. The diacetylide ligands adopt a *cis* coordination mode featuring non-planar terphenyl moieties as revealed by X-ray crystallographic analyses. The electrochemical, photophysical and photochemical properties of these platinum(II) complexes have been investigated. These platinum(II) diimine complexes show broad emission with peak maxima from 566 nm to 706 nm, with two of them having emission quantum yields

> 60% and lifetimes < 2 μ s in solutions at room temperature, whereas the platinum(II) diacetylide complexes having bis-*N*-heterocyclic carbene instead of diimine ligand display photoluminescence with quantum yields of up to 28% in solutions and excited state lifetimes of up to 62 μ s at room temperature. Application studies revealed that one of the complexes can catalyze photoinduced aerobic dehydrogenation of alcohols and alkenes, and a relatively non-toxic water-soluble Pt(II) complex displays anti-angiogenic activity.

Introduction

The use of acetylide ligands to boost the emission quantum yield is a milestone in the development of luminescent organo-platinum(II) complexes. In 1994, Che and co-workers reported the use of arylacetylide as a strong σ -donor ligand to prepare the first example of platinum(II) diimine bis-acetylide complex, [Pt(phen)(C \equiv CPh)₂] (phen = 1,10-phenanthroline).^[1] This complex in degassed solution displays a broad emission centred at 578 nm with 2.1 μ s lifetime that is assigned to originate from triplet metal-to-ligand charge transfer [$d\pi(\text{Pt}) \rightarrow \pi^*(\text{phen})$] (³MLCT) excited state. Since then, the use of acetylide ligands to prepare luminescent platinum(II) complexes has received a

surge of interest,^[2] and the application studies of these complexes in areas such as OLED,^[2c] energy up-conversion^[3b] and optical power limiting have been reported.^[3a] Subsequent works on platinum(II) acetylide complexes supported by tridentate ligand such as CNN (HCNN=6-phenyl-2,2'-bipyridine) and 2,2':6',2"-terpyridine by Che, Yam, Wu, Tung, Eisenberg and their co-workers have revealed the rich photo-physics and photochemistry of platinum(II) acetylide complexes.^[4,5]

Although numerous platinum(II) diimine complexes bearing monodentate acetylide ligands have been reported, platinum(II) diimine complexes bearing bidentate diacetylide ligands are relatively sparse in the literature with the first example reported by Castellano in 2006.^[6a] The platinum(II) diimine diacetylide complex Pt(dbbpy)(tda) (dbbpy = 4,4'-di-*tert*-butyl-2,2'-bipyridine, tda = tolan-2,2'-diacetylide) exhibits higher emission quantum yield and smaller non-radiative decay rate constant compared to the phenylacetylide counterpart, which reveals the superiority of employing a rigid cyclic diacetylide ligand.^[6a] In 2018, Yam and co-workers reported a series of platinum(II) diimine diacetylide complexes which underwent self-assembly and displayed near-infrared emission.^[6c] Apart from diimine ligands, Castellano and co-workers reported a Pt(II) diphosphine diacetylide complex displaying ligand-centred phosphorescence.^[7a] Wolf and co-workers prepared similar Pt(II) diphosphine metallacycles with thiophene-containing diacetylide ligands, with two of them showing room-temperature dual emission (fluorescence and phosphorescence).^[7b] This type of diacetylide ligands have also been used to prepare dinuclear platinum(II) complexes that exhibit reversible folding behavior in solution and supramolecular self-assembly, as well as dinuclear palladium(II) complexes displaying triplet metal-metal-to-ligand charge transfer (MMLCT) excited state.^[8,9] Recently, Wenger employed terphenyl diisocyanides as *cis*-

[a] Z. Luo

Department Key Laboratory of Pesticide & Chemical Biology
Ministry of Education and Chemical Biology Center
College of Chemistry
Central China Normal University
Wuhan 430079 (P. R. China)

[b] Dr. Y. Liu, Dr. X.-Y. Chang, Prof. Dr. C.-M. Che

Department of Chemistry
Southern University of Science and Technology
Shenzhen, Guangdong 518055 (P. R. China)
E-mail: cmche@hku.hk

[c] Dr. K.-C. Tong, Dr. W.-P. To, Prof. Dr. C.-M. Che

State Key Laboratory of Synthetic Chemistry
HKU-CAS Joint Laboratory on New Materials
Department of Chemistry
The University of Hong Kong
Pokfulam Road, Hong Kong SAR (P. R. China)
E-mail: kevintwp@hku.hk

[d] Prof. Dr. C.-M. Che

HKU Shenzhen Institute of Research and Innovation
Shenzhen, Guangdong 518057 (P. R. China)



Supporting information for this article is available on the WWW under
<https://doi.org/10.1002/asia.202100756>



This manuscript is part of a special collection on Metals in Functional Materials and Catalysis.

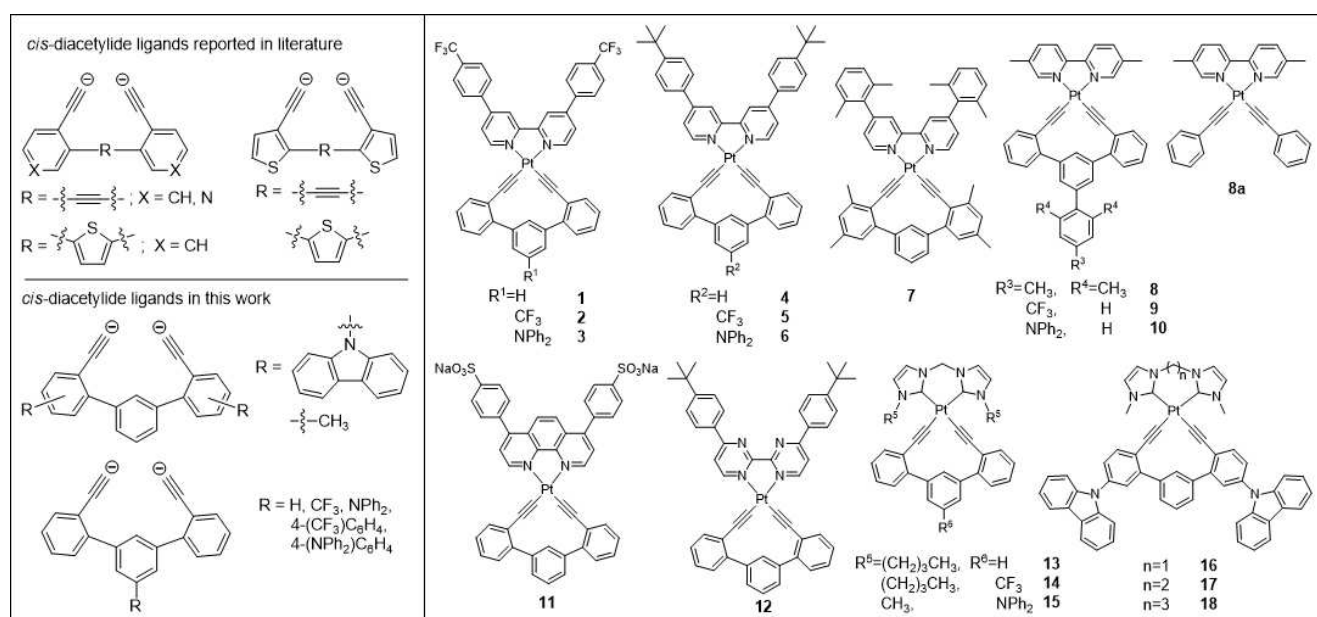
chelating ligand to prepare luminescent homoleptic Mo(0), Ni(0) and Cr(0) diisocyanide complexes.^[10] In this work we employed the isostructural terphenyl diacetylides to prepare a series of charge-neutral luminescent platinum(II) diimine and bis-*N*-heterocyclic carbene complexes. The electrochemical, photophysical and photochemical properties of these platinum(II) complexes have been investigated.

Results

Synthesis and characterization: The chemical structures of complexes 1–18 are shown in Scheme 1. The syntheses of these new diacetylenes are described in the Supporting Information. Complexes 1–18 and some of the diimine ligands were prepared according to the reported procedures as described in the Experimental Section and Supporting Information. Platinum(II) diimine complexes with diacetylides (1–12) were prepared in 50–85% yields by the reaction of [Pt(NN)Cl₂] (NN = 2,2'-dipyridyl or 2,2'-bipyrimidine or 1,10-phenanthroline derivatives) with the diacetylene in DMF or CH₂Cl₂ in the presence of *i*Pr₂NH and a catalytic amount of CuI.^[2c,11] Complexes 1–6 and 11 precipitated from the reaction mixture and were isolated by filtration, while complexes 7–10 and 12 were obtained by chromatography on SiO₂ column. Complexes 13–15 were synthesized by treating [Pt(bis-NHC)Cl₂] with the diacetylene in DMF in the presence of *i*Pr₂NH and a catalytic amount of CuI. Complexes 16–18 were prepared by treating the precursor [Pt(COD)(C≡C–Ar–C≡C)] (C≡C–Ar–C≡C represents diacetylide) with imidazolium salt in DMF in the presence of NaOAc under reflux with yields of 40–57%. These bis-NHC complexes were purified by column chromatography. All complexes were characterized by ¹H NMR spectroscopy, infrared spectroscopy, mass spectrometry and elemental analyses. ¹³C NMR spectra were obtained only for 7,

12–14 because of solubility reason. Only one ν(C≡C) stretching was found at 2109–2136 cm⁻¹ for these complexes, similar to that observed in Pt(II) diphosphine diacetylide complex.^[7b] All these complexes show no sign of decomposition upon storage for a few months in the solid state and are stable in solutions for at least a few days under ambient conditions in the absence of light. As to their photostability, when complexes 2, 8 and 12 were subjected to 410 nm LED irradiation in degassed [D₆] DMSO, CD₂Cl₂ and CDCl₃, respectively, for 24 hours, only minor change was observed in their corresponding ¹H NMR spectrum (Figure S1, S2 and S4). The counterpart complex of 8 with two monodentate phenylacetylide (8a) was also prepared according to the reported procedure for comparison.^[2c] Under the same conditions, 8a showed significant decomposition after 24 hours as revealed in ¹H NMR spectroscopy (Figure S3), indicating the improved stability of platinum complex supported by diacetylide ligand. Complex 7 has a good solubility in DMSO, CH₃OH, CH₃CN, CHCl₃ and CH₂Cl₂. Complex 11 has a good water solubility due to the sulfonate groups on the diimine ligand.

Crystal structures: The structures of 7, 8, 10 and 13 (Figure 1) have been characterized by single crystal X-ray crystallography. The crystals were obtained by slow diffusion of diethyl ether into dichloromethane solution of 7, 8, 10 and 13, respectively. Crystallographic data and selected bond lengths and angles for 7, 8, 10 and 13 are listed in Table S3 and Table S4, respectively. All the Pt atoms show a distorted planar geometry similar to those reported for other diimine bis(arylalkynyl)-platinum(II) complexes.^[2] The Pt–N (2.054–2.069 Å) and Pt–C (1.935–1.954 Å) bond lengths and N–Pt–N (78.59–79.92°) and C–Pt–C (83.93–84.93°) bond angles of 7, 8 and 10 are in the range commonly found in similar Pt(II) complexes.^[2] The Pt–N bonds are slightly longer than those of the [Pt-(diimine)Cl₂] (1.992–2.015 Å), presumably due to the *trans* effect of the carbon donor ligands. The Pt–C bond lengths



Scheme 1. Chemical structures of *cis*-diacetylide ligands (left) and complexes 1–18 and 8a (right).

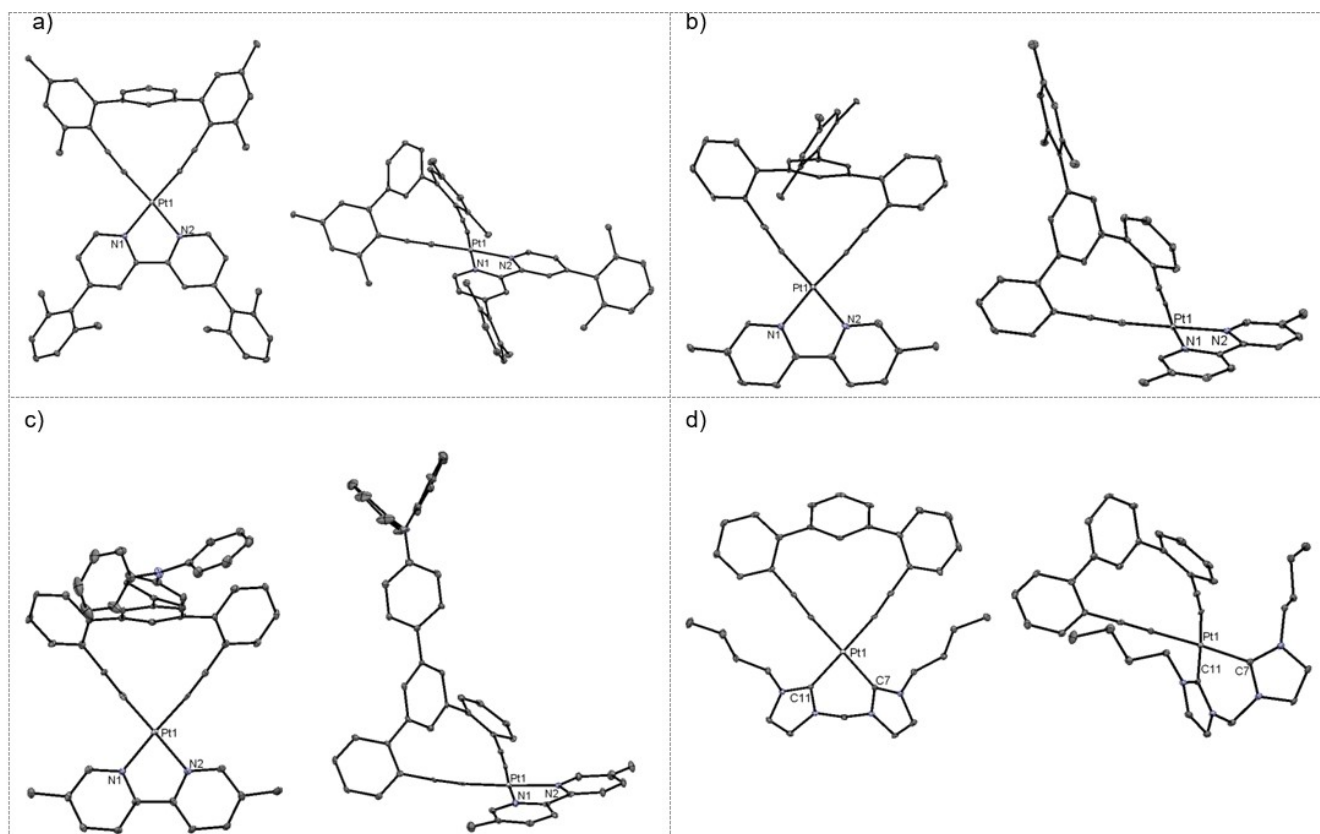


Figure 1. Perspective views of complexes (a) 7, (b) 8, (c) 10 and (d) 13.

range from 1.935 to 1.954 Å and are similar to those reported for platinum(II) diimine bis(acetylide) complexes.^[2] The $C_{alkynyl}-Pt-C_{alkynyl}$ bond angles are similar (84.36° for 7, 84.93° for 8, 83.93° for 10), being much smaller than that of platinum(II) diimine bis(arylacetylide) complexes (88.83°),^[2] which may be ascribed to the rigidity of terphenyl diacetylides. The bond lengths of $Pt-C_{carbene}$ (2.016–2.022 Å) and $Pt-C_{alkynyl}$ (1.991–1.994 Å) of 13 are in the same order as those of the platinum(II) acetylide complexes bearing NHC ligands.^[12] The bond angles of $C_{alkynyl}-Pt-C_{alkynyl}$ (84.28°) of 13 are smaller in comparison with the reported platinum(II) acetylide complexes bearing bis-NHC ligands ($87.9-88.8^\circ$).^[12a] Complexes 7, 8 and 10 show intermolecular metal- π interaction between Pt and the diimine moiety in their crystal structures (distance between [Pt(NN)] planes: 3.597 Å for 7, 3.456 Å for 8, 3.371 Å for 10; Figure S6–S8), while for 13, only C–H $\cdots\pi$ interactions (2.552–2.750 Å) between the protons on the bis-NHC ligand and diacetylide ligand were observed (Figure S9). The terphenyl diacetylide ligands in these crystal structures adopt a non-planar conformation analogous to that of terphenyl diisocyanide counterparts in $Mo(CNAr_3NC)_3$ ($CNAr_3NC = 2,2''$ -diisocyanato-3,5,3'',5''-tetramethyl-1,1':3',1''-terphenyl).^[10] For example, a large dihedral angle of 71.1° between the central phenyl ring of the terphenyl moiety and the [Pt(NN)] moiety is observed in 8 (Figure S5), and such dihedral angle increases to 80.0° in 10 which has a bulkier *p*-(diphenylamino)phenyl substituent on the central phenyl ring. Additional insight on the intermolecular interactions in the

crystal structures of 7, 8, 10 and 13 could be gained by the constructions of their corresponding Hirshfeld surfaces.^[13] The Hirshfeld surfaces mapped with d_{norm} and d_e of 8 are displayed in Figure 2 and those of 7, 10 and 13 in Figures S10–S12. The cavities generated by the mesityl (8) and triphenylamine (10) moieties on the twisted triphenyl hinge introduce the capability

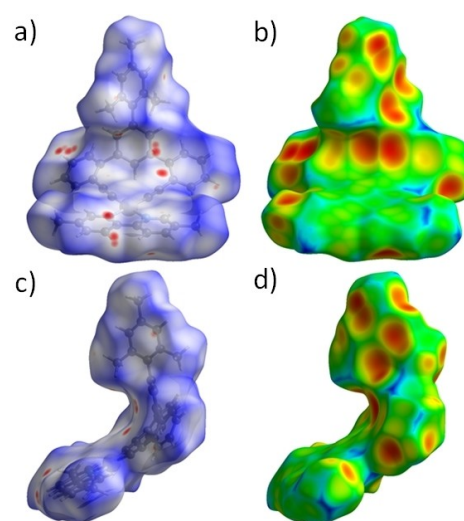


Figure 2. Hirshfeld surface of 8 view from concave side mapped with (a) d_{norm} and (b) d_e , and lateral view mapped with (c) d_{norm} and (d) d_e .

for significant close intermolecular interactions. In contrast, the central phenyl ring of **7** and **13** show weak and moderate intermolecular interactions.

Absorption Spectroscopy: The absorption data of all the complexes are recorded at room temperature and the data are summarized in Table 1. UV/Vis absorption spectra of **1–3** and **6** in dichloromethane are shown in Figure 3. Complexes **1–6** show intense absorption bands at 250–370 nm ($\epsilon > 10^4 \text{ dm}^3 \text{ mol}^{-1} \text{ cm}^{-1}$) that are assigned to the intraligand (¹IL) transition of the diimine and/or diacetylde ligands. The UV/Vis

absorption spectra of **1–6** show low-energy absorption bands in the range of 390–480 nm and these are assigned as predominant singlet metal-to-ligand charge transfer (MLCT) $^1[5d_{z^2}(\text{Pt}) \rightarrow \pi^*(\text{diimine})]$ transitions. We note that the low-energy transitions for complexes **1–6** appear at 433–459 nm, which are significantly red-shifted in comparison with that for $[\text{Pt}(4,4'\text{-diphenyl-2,2'}\text{-bipyridine})(\text{C}\equiv\text{CPh})_2]$ (411 nm).^[2c] This can be attributed to stronger σ -donation by diacetylde ligands resulting in destabilization of metal-based HOMO. Compared with **4**, the low-energy absorption peak maximum of **1** is red-shifted

Table 1. Photophysical properties of complexes **1–18**.^[a]

	UV/Vis absorption ^[b] λ_{max} [nm] (ϵ [$10^3 \text{ dm}^3 \text{ mol}^{-1} \text{ cm}^{-1}$])	Emission Solution, 293 K ^[b] λ_{max} [nm] (Φ [%] ^[h] ; τ [μs]; k_r [10^4 s^{-1}]; k_{nr} [10^4 s^{-1}])	Solid, 293 K λ_{max} [nm] (τ [μs])	Solid, 77 K λ_{max} [nm] (τ [μs])	Glassy, 77 K ^[i] λ_{max} [nm] (τ [μs])
1	292 (42.6, sh), 311 (37.0, sh), 347 (11.8, sh), 424 (9.7, br, sh), 459 (11.2, br)	628 (6.1; 0.27; 22.6; 348)	692 (0.41)	709 (0.70)	553 (3.7), 590 (sh)
2	288 (34.8, br), 312 (30.5, sh), 350 (9.2, br, sh), 420 (8.1, br, sh), 454 (9.7, br)	616 (14; 0.58; 24.1; 148)	688 (0.35)	686 (1.0)	541 (3.3), 580 (sh)
3	255 (52.0, sh), 297 (40.8), 317 (33.6, sh), 355 (8.2, br, sh), 448 (7.8, br)	Non-emissive	580 (0.35), 616 (sh)	585 (3.1), 635	580 (3.2), 627
4	273 (38.7), 305 (39.7), 420 (10.0, br, sh), 442 (10.4, br)	600 (18; 0.61; 29.5; 134)	549 (sh), 577 (0.17), 630 (sh)	548 (2.1), 590, 637 (sh)	545 (2.1), 588, 633 (sh)
	273 (37.0), 305 (37.7), 423 (7.9, br, sh), 460 (9.3, br) ^[c] 308 (41.7), 411 (10.5, br, sh), 433 (11.3, br) ^[d]	603 (3.5; < 0.1; N.A.) ^[c] 596 (3.5; 0.14; 25.0; 689) ^[d]	535 (0.40), 561, 614 (sh)	534 (1.9), 578, 617 (sh)	532 (3.0), 568, 622 (sh)
5	273 (42.8), 306 (44.1), 334 (26.3, sh), 418 (10.7, br, sh), 440 (11.8, br)	588 (31; 0.95; 32.6; 72.6)	548 (0.25), 579 (sh)	543 (1.9), 587, 635 (sh)	529 (2.4), 570, 615 (sh)
6	276 (56.8), 305 (69.1), 433 (14.5, br)	611 (0.7; < 0.1; N.A.)	548 (0.25), 579 (sh)	543 (1.9), 587, 635 (sh)	529 (2.4), 570, 615 (sh)
7	297 (31.2), 416 (6.6, br, sh), 455 (7.2, br) 344 (7.4), 494 (5.7) ^[e]	630 (3.0; 0.10; 30.0; 970) 629 (4.8; 0.12; 40.0; 793) ^[e]	575 (0.27), 616	560 (2.3), 601	527 (3.4), 559
8	273 (34.1, sh), 305 (34.6), 330 (12.4, sh), 407 (8.6, br), 429 (8.1, sh)	572 (64; 1.43; 44.8; 25.2)	667 (0.58)	688 (1.2)	489 (3.5), 523, 563 (sh)
9	270 (43.9), 303 (33.3), 405 (7.8), 425 (7.1, br, sh)	566 (71; 1.58; 44.9; 18.4)	522 (0.18), 550	529 (0.70), 563, 598 (sh)	487 (3.1), 520, 563 (sh)
10	306 (55.9), 340 (37.9, sh), 402 (9.4, br), 426 (8.3, br, sh)	570 (35; 0.90; 38.9; 72.2)	612 (0.30)	634 (1.3)	488 (3.1), 520, 562 (sh)
11	286 (38.3), 400 (7.0, br), 428 (6.2, br, sh) ^[f] 288 (35.5), 416 (5.2, br) ^[g]	609 (3.5; 0.22; 15.9; 439) ^[f] 570, 706 (1.2; $\tau_{570} = 0.4$, $\tau_{706} = 0.3$; n.a.) ^[g]	706 (0.30)	716 (2.4)	526 (6.3), 563, 613 (sh)
12	264 (36.4), 296 (35.9, sh), 309 (34.8), 365 (14.6, sh), 434 (7.9, br), 525 (1.4, tail)	627 (2.0; < 0.1; N.A.)	592 (0.14), 631 (sh)	579 (1.0), 630, 688 (sh)	543 (2.9), 576, 621 (sh)
13	256 (44.7), 283 (22.9), 328 (25.2, br), 340 (23.2, br, sh)	458 (3.4; 2.7; 1.3; 35.8), 482 (sh)	470 (0.54), 486	470 (25.5), 511	448 (44.0), 476
14	253 (41.2), 283 (20.0), 328 (24.7), 341 (21.3, sh)	462 (4.1; 4.0; 1.0; 24.0), 485 (sh)	467 (sh), 533 (2.6)	472 (sh), 528 (54.5)	477 (58.4)
15	258 (32.6), 288 (25.9), 327 (24.1, br), 348 (16.2, br, sh)	463 (5.4; 4.1; 1.3; 23.1), 492 (sh)	466 (sh), 523 (0.36)	483 (sh), 530 (7.2)	461 (42.2), 487, 525 (sh)
16	258 (56.6, sh), 294 (35.7), 330 (30.2, br, sh), 348 (32.9, br)	477 (26; 28.0; 0.9; 2.6), 510 (sh)	495 (2.3)	505 (44.3)	466 (54.5), 497
17	293 (48.5), 324 (44.7), 340 (41.9)	477 (23; 22.1; 1.0; 3.5), 503 (sh)	523 (1.29)	503 (24.1)	464 (84.6), 497, 550 (sh)
18	294 (48.2), 315 (40.8, br), 332 (36.9, br, sh) 293 (52.4), 313 (40.0, br), 341 (31.0, br, sh) ^[c] 294 (47.2), 316 (40.2, br), 339 (33.8, br, sh) ^[d] 295 (51.9), 318 (42.3, br), 332 (40.1, br, sh) ^[e]	478 (sh), 508 (27; 42.6; 0.6; 1.7) 482 (sh), 507 (16; 62.0; 0.3; 1.4) ^[c] 482 (sh), 508 (19; 58.3; 0.3; 1.4) ^[d] 478 (sh), 502 (28; 48.4; 0.6; 1.5) ^[e]	467 (sh), 492 (2.2)	499 (42.0)	465 (92.1), 496

[a] Abbreviations: ϵ = extinction coefficient; Φ = quantum yield; τ = lifetime; k_r (radiative decay rate constant) is estimated by $k_r = \Phi/\tau$; k_{nr} (non-radiative decay rate constant) is estimated by $k_{nr} = (1-\Phi)/\tau$. [b] Determined in degassed CH_2Cl_2 ($2.0 \times 10^{-5} \text{ mol dm}^{-3}$). [c] Determined in degassed THF ($2.0 \times 10^{-5} \text{ mol dm}^{-3}$). [d] Determined in degassed DMF ($2.0 \times 10^{-5} \text{ mol dm}^{-3}$). [e] Determined in degassed toluene ($2.0 \times 10^{-5} \text{ mol dm}^{-3}$). [f] Determined in degassed CH_3OH ($2.0 \times 10^{-5} \text{ mol dm}^{-3}$). [g] Determined in degassed H_2O ($2.0 \times 10^{-5} \text{ mol dm}^{-3}$). [h] Using quinine sulfate in 0.5 M H_2SO_4 ($\Phi_{\text{em}} = 0.546$) as reference. [i] $\text{CH}_2\text{Cl}_2/\text{MeOH}/\text{EtOH}$ (v/v/v) = 1:1:4 at 77 K.

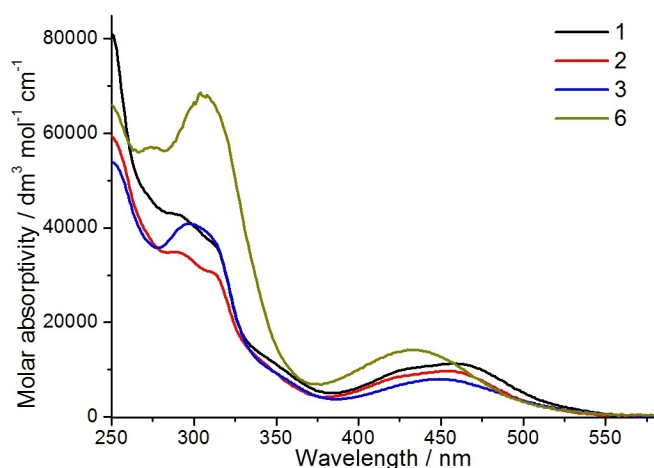


Figure 3. UV/Vis absorption spectra of 1–3 and 6 in CH₂Cl₂ at room temperature.

(442 to 459 nm) attributed to the presence of electron-withdrawing trifluoromethyl groups on the diimine ligands. The low-energy absorption band of 4 shows negative solvatochromism (λ_{max} : 460 nm in THF, 442 nm in CH₂Cl₂, 433 nm in DMF; Figure S19). The UV/Vis absorption spectra of complexes 8, 10 and 12 in CH₂Cl₂ are shown in Figure 4 and that of 11 in MeOH and H₂O in Figure 5. On moving from 8–10, the low-energy absorption bands show a slight blue-shift ($407 < 405 < 402$ nm) presumably because the substituent(s) (CF₃, NPh₂) on the diacetylide ligands are remote from the main terphenyl diacetylide scaffold and hence does not exert notable influence on the ¹MLCT transition. Complex 10 shows an absorption band ($\epsilon = 5.58 \times 10^4$ dm³ mol⁻¹ cm⁻¹) at 306 nm which is more intense than those of 8–9, and this may be attributed to the contribution of the diphenylamino substituent. Complexes 11 and 12 also show low-energy absorption bands which are assigned as ¹MLCT transitions. The absorption of 12 is significantly red-shifted compared to those of 1–10 due to the use of substituted 2,2'-bipyrimidine which gives rise to a LUMO that is lower-lying than complexes with substituted 2,2'-bipyridine (1–10). The UV/Vis absorption spectra of the bis-NHC

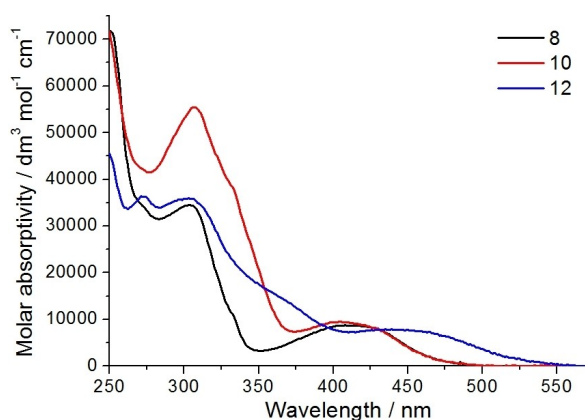


Figure 4. UV/Vis absorption spectra of 8, 10 and 12 in CH₂Cl₂ at room temperature.

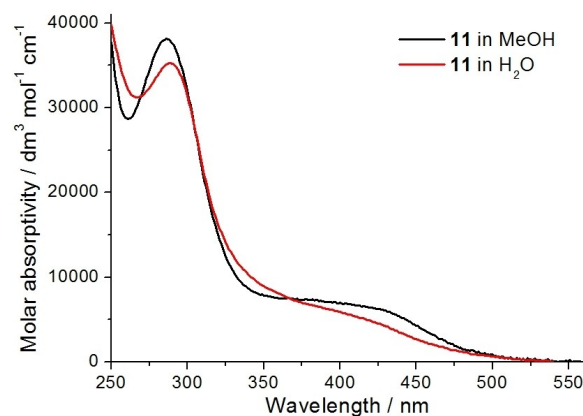


Figure 5. UV/Vis absorption spectra of 11 in MeOH and H₂O at room temperature.

complexes 13, 15, 16, 18 in CH₂Cl₂ are shown in Figure 6. Complexes 13–18 show low-energy absorption bands in the range of 310–390 nm, which are assigned to a mixture of singlet intraligand (¹IL) [$\pi(\text{alkynyl}) \rightarrow \pi^*(\text{alkynyl})$] and metal-to-ligand charge transfer (¹MLCT) [$5d_{22}(\text{Pt}) \rightarrow \pi^*(\text{alkynyl})$] transitions. The high-energy absorption bands (<310 nm) of 13–18 are assigned to ¹IL [$\pi(\text{alkynyl}) \rightarrow \pi^*(\text{alkynyl})$] transitions. For complexes 16–18, their low-energy absorption bands show a gradual blue-shift in the order of 16 (348 nm) > 17 (340 nm) > 18 (332 nm) when the length of linker between the two *N*-heterocyclic carbene ligating groups is increased. The low-energy absorption band of complex 16 (348 nm) show obvious red-shift compared with that of 13 (340 nm), which could be due to the presence of electron-rich carbazole moieties on the diacetylide ligand of 16.

Emission Spectroscopy: The emission data of all the complexes are shown in Table 1 and their emission spectra in Figure 7–10 and Table S1. Complexes 1, 2, 4–10 and 12 display a structureless, broad emission band in degassed dichloromethane solutions at room temperature; 3 is non-emissive under the same condition. With reference to previous works on platinum(II) diimine bis(acetylide) complexes,^[2] the origin of the emission bands of complexes 1, 2, 4–10 and 12 are assigned as ³MLCT [$5d_{22}(\text{Pt}) \rightarrow \pi^*(\text{diimine})$] excited state. The emission λ_{max} of

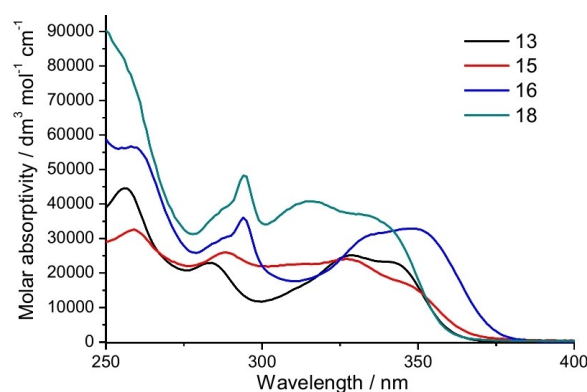


Figure 6. UV/Vis absorption spectra of 13, 15, 16 and 18 in CH₂Cl₂ at room temperature.

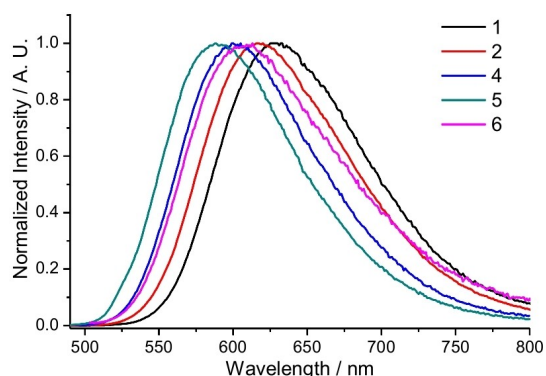


Figure 7. Emission spectra of Pt(II) diimine complexes **1**, **2**, **4**, **5** and **6** in CH_2Cl_2 ($2.0 \times 10^{-5} \text{ mol dm}^{-3}$) at room temperature.

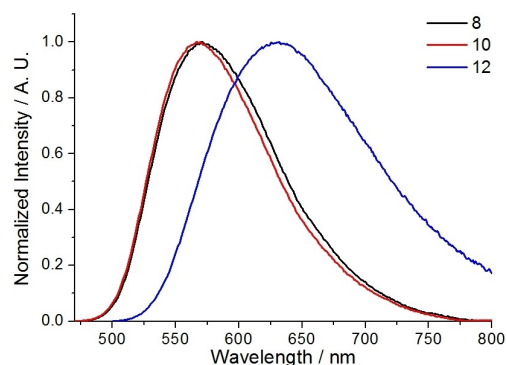


Figure 8. Emission spectra of Pt(II) diimine complexes **8**, **10** and **12** in CH_2Cl_2 ($2.0 \times 10^{-5} \text{ mol dm}^{-3}$) at room temperature.

1, **2**, **4**–**6** are at 588–628 nm and their radiative decay rate constants (k_r) are on the order of 10^5 s^{-1} , consistent with the significant metal parentage in the emissive excited state. The emission λ_{max} of **4** shows minimal variation in different solvents (600 nm in CH_2Cl_2 , 603 nm in THF, 596 nm in DMF) (Table 1). The slight blue-shift in λ_{max} of **4** upon changing the solvent from CH_2Cl_2 (600 nm) to DMF (596 nm) is in accord with that reported for $[\text{Pt}(\text{diimine})(\text{C}\equiv\text{CAr})_2]$ system (Figure S20).^[2c] The emission λ_{max} of **4**–**6** show a red-shift in the order of 5 (588 nm) < **4** (600 nm) < **6** (611 nm), which can be accounted for by the increasing electron-donating strength of the substituent on the diacetylde (**5** with CF_3 , **4** with H, **6** with NPh_2).^[2a] The λ_{max} of **1** (628 nm) and **2** (616 nm) show a notable red-shift compared with **4** (600 nm) and **5** (588 nm) because of the electron-withdrawing CF_3 groups on the bipyridine ligand of **1**–**2**, which reduce the energy gap between $5d_{z^2}(\text{Pt})$ and $\pi^*(\text{diimine})$ orbitals. Complexes with electron-donating NPh_2 substituent (**3**, **6**) show inferior luminescence compared with those with other substituents (**1**, **2**, **4**, and **5**). Related observation has also been reported by Eisenberg and co-workers in which the $[\text{Pt}(\text{diimine})(\text{C}\equiv\text{CAr})_2]$ complex with 4-methoxyphenylacetylde ligands shows the lowest emission quantum yield among other complexes with arylacetylde ligands having less electron-donating substituents.^[2a] The emission spectra of complexes **8**, **10**, **12** in CH_2Cl_2 are shown in Figure 8. For **8**–**10**, their emission λ_{max} differ by only 185 cm^{-1} presumably because they have the same diimine ligand and the substituents on the diacetylde ligand are remote from the chromophoric moieties and thus have little effect on the $[5d_{z^2}(\text{Pt}) \rightarrow \pi^*(\text{diimine})]$ excited state. The emission quantum yields of complexes **8**–**10** (35–71%) are much higher than that of **1**–**6** (0.7%–31%) which may be ascribed to the use of 5,5'-dimethyl-2,2'-bipyridine (5MeBpy) in **8**, **9** and **10**. The non-radiative decay rate constants (k_{nr}) of **8**, **9** and **10** are in the range of 1.8 – $7.2 \times 10^5 \text{ s}^{-1}$, which are in general smaller than those of **1**, **2**, **4** and **5** (k_{nr} : 7.3 – $34.8 \times 10^5 \text{ s}^{-1}$). These observations are consistent with the literature where the $[\text{Pt}(\text{diimine})(\text{C}\equiv\text{CAr})_2]$ complex with 5MeBpy shows the highest emission quantum yield among the series.^[2c] Emission of **11** was measured in methanol and H_2O instead of CH_2Cl_2 as the

presence of two sulfonate groups on the diimine ligand of **11** renders this complex insoluble in CH_2Cl_2 . This complex shows luminescence with λ_{max} at 609 nm and quantum yield of 3.5% in methanol (Figure 9). When it is dissolved in H_2O , it displays two broad emission bands with λ_{max} at 570 and 706 nm with 1.2% emission quantum yield. The slightly different excitation spectral profiles recorded at these emission λ_{max} suggest that these two emission bands may originate from different excited states/species (Figure S21). Since the emission λ_{max} at 706 nm is the same as **11**'s solid state emission λ_{max} , this low-energy emission might originate from nano-aggregate species of **11**. Light scattering analysis of an aqueous solution of **11** ($2 \times 10^{-5} \text{ M}$) revealed the presence of nanoparticles with size of $\sim 120 \text{ nm}$, supportive of the formation of aggregate species (Figure S22). Thus, the emission band with λ_{max} at 570 nm is assigned as $^3\text{MLCT}$ emission while that at 706 nm is assigned as emission from nano-aggregates of **11** in water.

The emission spectra of Pt(II) bis-NHC complexes **13**, **15**, **16**, **18** in CH_2Cl_2 are shown in Figure 10. Complexes **13**–**18** exhibit a broad emission band but with a slightly vibronic structure. With carbazole on the arylethynyl moieties, complexes **16**–**18** display enhanced luminescence with λ_{max} of 477–510 nm which are red-shifted compared with complexes **13**–**15** (458–492 nm). Importantly, complexes **16**–**18** show emission quantum yields of 23–27% and long lifetimes of 22.1–42.6 μs in degassed

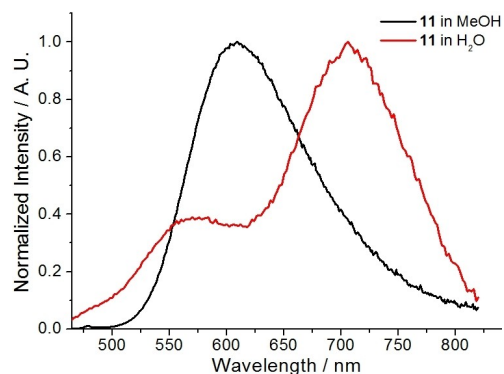


Figure 9. Emission spectra of **11** in MeOH and H_2O ($2.0 \times 10^{-5} \text{ mol dm}^{-3}$) at room temperature.

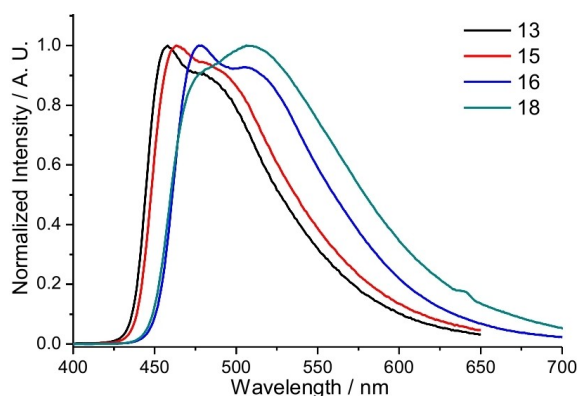


Figure 10. Emission spectra of Pt(II) bis-NHC complexes **13**, **15**, **16** and **18** in CH_2Cl_2 ($2.0 \times 10^{-5} \text{ mol dm}^{-3}$) at room temperature.

CH_2Cl_2 , corresponding to k_r of $0.6\text{--}1.0 \times 10^4 \text{ s}^{-1}$ that is one order of magnitude smaller than that of **1–12**. Considering the vibronically structured emission profile and much smaller k_r , the emission of **13–18** are assigned to originate predominantly from metal-perturbed $^3\text{IL} [\pi(\text{alkynyl}) \rightarrow \pi^*(\text{alkynyl})]$ excited states. With reference to previous studies, the attachment of bulky *N*-carbazolyl groups to the [Pt(ONCN)] or [Pt(OCCO)] complexes has been found to exert a significant effect on the emissive excited states, as well as result in a significant suppression of intermolecular interactions.^[14] For comparison, [(pim)Pt(C \equiv R) $_2$] (pim = 1,1'-dipentyl-3,3'-methylene-diimidazole-2,2'-diylidene) complexes were reported to show emission quantum yields in range of 0.2%–3.4% and lifetimes of up to 29 μs .^[12a] Platinum(II) complexes bearing bis-carbene and deprotonated 2-arylpiperidine as cyclometalating ligand show strong luminescence (quantum yield = 5%–54%) with λ_{max} at 477–550 nm in solutions at room temperature and with 1.4–42 μs lifetime.^[15] Remarkably, for these reported complexes, the aliphatic chain linking the two NHC moieties has notable influence on the luminescence properties. When the aliphatic chain length increases from $-(\text{CH}_2)-$ to $-(\text{CH}_2)_3-$, the emission quantum yields and lifetimes of these complexes increase due to a significant reduction of k_{nr} (from $68 \times 10^4 \text{ s}^{-1}$ to $1.7 \times 10^4 \text{ s}^{-1}$, and from $15 \times 10^4 \text{ s}^{-1}$ to $1.1 \times 10^4 \text{ s}^{-1}$), with the complex bearing $(\text{CH}_2)_3$ -bridged bis-NHC ligand showing a high emission quantum yield (54%) in solution at room temperature and a long lifetime of 42 μs (complex **3b** PF_6 in their work) as well as a blue-shift (10–12 nm) in emission λ_{max} .^[15a] In this work, we note that there is only a minor difference in emission λ_{max} of **16–18** (477 and 510 nm for **16**; 477 and 503 nm for **17**; 478 and 508 nm for **18**) and a minor variation in emission quantum yields (23–27%) when the linker length of the bis-NHC is increased from $-(\text{CH}_2)-$ as in **16** to $-(\text{CH}_2)_3-$ as in **18**. The λ_{max} of **18** shows minimal variation in different solvents (478 and 508 nm in CH_2Cl_2 , 478 and 502 nm in toluene, 482 and 507 nm in THF, 482 and 508 nm in DMF) (Table 1). The much improved emission quantum yields of **16–18** compared with **13–15** highlight that the substituent on diacetylde ligand could have a drastic impact on luminescent properties.

The emission of **1–18** in the solid state at 293 K and 77 K and in $\text{CH}_2\text{Cl}_2/\text{MeOH}/\text{EtOH}$ (1:1:4 v/v/v) at 77 K were also measured. The emission spectra of **4** recorded under these conditions are shown in Figure 11. Complexes **1–12** exhibit yellow to red emission with λ_{max} at 522–706 nm in the solid state at room temperature and at 529–716 nm in the solid state at 77 K. The emission quantum yields of **1**, **4**, **7** and **8** in the solid state at room temperature are 27%, 5%, 12% and 35%, respectively, implying k_r of $2.9\text{--}6.6 \times 10^5 \text{ s}^{-1}$. In glassy solutions at 77 K, these complexes exhibit structured emission with λ_{max} at 487–627 nm akin to reported Pt(II) diimine arylacetylde complexes.^[2c] The vibrational progression spacings for these vibronic structured emissions range from 1060 to 1360 cm^{-1} , which can be assigned to stretching vibration of the polypyridyl ligand and/or terphenyl moiety of the diacetylde ligand. For Pt(II) bis-NHC complexes **13–18**, they exhibit blue-green to yellow emission with λ_{max} at 470–530 nm in the solid state at 293 K and λ_{max} at 470–530 nm in the solid state at 77 K. Complexes **13**, **15–18** exhibit structured emission with λ_{max} at 448–497 nm in glassy solution at 77 K while complex **14** displays a structureless emission band centred at 477 nm with FWHM of 75 nm. The vibrational progression spacing of **16** is estimated to be 1470 cm^{-1} , and can be assigned to skeletal vibration localized on the diacetylde ligand.

Ultrafast time-resolved absorption and emission spectroscopy: The excited state dynamics of complexes **1**, **4**, **10**, **13** and **18** have been examined with femtosecond (fs) and nanosecond (ns) time-resolved absorption difference (TA) spectroscopy. fs-TA measurements for **1**, **4**, **10** were conducted with excitation at 400 nm in DMF while those for **13** and **18** were conducted with excitation at 266 nm in CH_2Cl_2 solutions. The fs-TA spectra of the Pt(II) diimine complexes **1** and **4** display a broad absorption difference band at 530–650 nm right after excitation at 400 nm, which showed little change within 2 ns (Figure 12 and S23). For **10**, a weak TA band at ~ 460 nm and a broad, strong band with shoulder at 550 nm and peak maximum at ~ 630 nm right after laser excitation were recorded (Figure S24). This profile evolved with a time constant of 197 ps to another profile with TA maxima at ~ 450 , ~ 520 and ~ 630 nm. The ns-TA spectra of **1** and **4** in CH_2Cl_2 both show

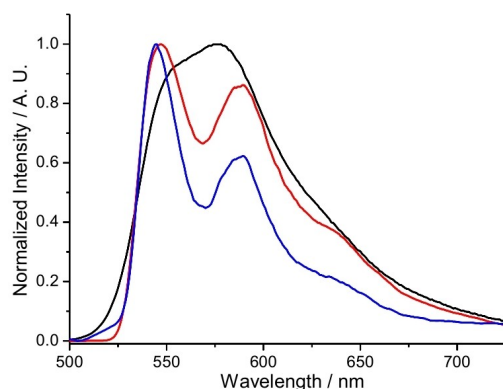


Figure 11. Emission spectra of **4** in the solid state at room temperature (black line) and 77 K (red line). Emission spectrum of **4** in $\text{CH}_2\text{Cl}_2/\text{MeOH}/\text{EtOH}$ (1:1:4 v/v/v) emission at 77 K (blue line).

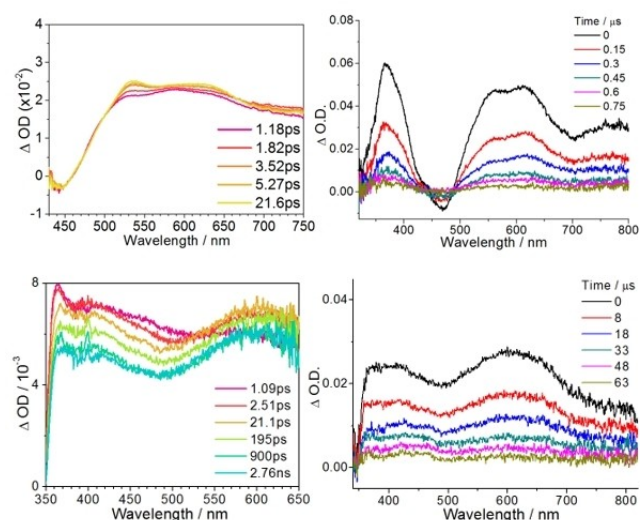


Figure 12. fs-TA (left) and ns-TA (right) spectra of **1** (upper) and **18** (lower) in solution at room temperature.

absorption difference peak maxima at ~ 370 nm and a broad band at 500–800 nm (Figure 12 and S23), the former of which can be assigned to the anion radical of the bipyridine moiety supportive of MLCT assignment.^[2b] The decay time constants of these signals are close to their respective emission lifetimes, suggesting that these ns-TA signals originate from their emissive excited states. The ns-TA spectrum of **10** in CH_2Cl_2 also shows a strong absorption difference peak at ~ 370 nm as well as a broad band with peak maximum at ~ 630 nm with decay time constant of 0.8 μs . The Pt(II) bis-NHC complexes **13** and **18** both display fs-TA absorption > 360 nm with profile similar to those of their ns-TA absorption difference spectra, implying that the intersystem crossing process is completed within 1 ps after laser excitation (Figure 12 and S25). Their ns-TA lifetimes (2.9 and 29 μs respectively) are comparable to their emission lifetimes, suggesting that these ns-TA signals arise from their emissive excited states.

Electrochemical properties: The cyclic voltammograms of complexes **1–18** have been recorded (except for **15** due to low solubility) and the data are listed in Table 2. The cyclic voltammograms of **1**, **12** and **14** are depicted in Figure 13 while others in Table S2. The voltammograms were measured in DMF using 0.1 M $[n\text{-Bu}_4\text{N}][\text{PF}_6]$ as supporting electrolyte, and ferrocenium/ferrocene (Fc^+/Fc) was used as an internal reference. In general, complexes **1–12** display one irreversible oxidation wave with E_{pa} at 0.87–1.24 V vs. SCE and one reversible reduction couple with E_{pc} at -0.95 to -1.38 V vs. SCE. Upon scanning to more negative potentials, complexes **1–7** display a quasi-reversible reduction couple with $E_{1/2}$ at -1.54 to -1.88 V and **8–12** an irreversible reduction wave with E_{pc} at -1.57 to -2.07 vs. SCE. The oxidation waves are assigned to oxidation of Pt(II) to Pt(III) and the reductions are assigned to ligand-centred reduction of the diimine ligands with reference to the literature.^[2] Complexes **1–3** show more anodic $E_{1/2}^{\text{red}}$ than **4–6** due to the presence of electron-withdrawing CF_3 groups on the

Complex	$E_{\text{pa}}^{[b]}$	$E_{\text{pc}}^{[b]}$	$E_{1/2}^{\text{red}}$
1	0.87	−1.09, −1.60	−1.06, −1.56
2	0.95	−1.08, −1.58	−1.05, −1.54
3	0.95	−1.09, −1.62	−1.06, −1.56
4	0.92	−1.22, −1.79	−1.19, −1.75
5	0.99	−1.21, −1.80	−1.18, −1.76
6	0.97	−1.22, −1.79	−1.19, −1.75
7	1.21	−1.26, −1.92	−1.23, −1.88
8	1.03	−1.38, −2.07	−1.35
9	0.93	−1.37, −2.06	−1.33
10	1.06	−1.37, −2.03	−1.34
11	1.24	−1.21, −1.81	−1.17
12	0.96	−0.95, −1.57	−0.92
13	1.12	–	–
14	1.21	−2.35	–
15^c	–	–	–
16	1.02	–	–
17	1.01	–	–
18	1.03	–	–

[a] Determined in DMF at room temperature with 0.1 mol dm^{-3} $n\text{-Bu}_4\text{NPF}_6$ as supporting electrolyte. Scanning rate: 100 mVs^{-1} . Values are versus SCE. $\text{Cp}_2\text{Fe}^{+/0}$ occurs at 0.48 V versus SCE reference electrode. [b] E_{pa} and E_{pc} denote the peak potentials of anodic and cathodic waves, respectively. [c] Cannot be determined due to low solubility.

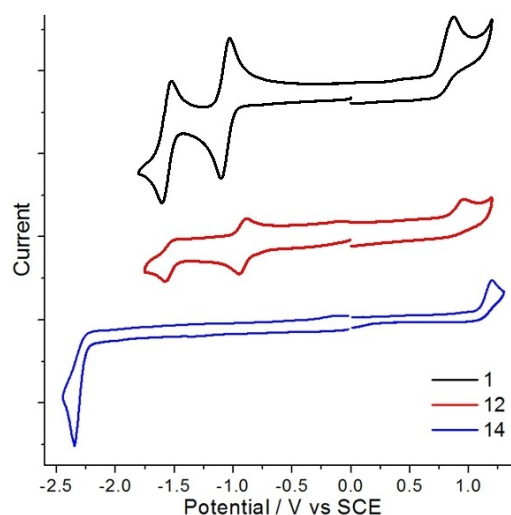


Figure 13. Cyclic voltammograms of **1**, **12** and **14** in DMF with 0.1 M $[n\text{-Bu}_4\text{N}][\text{PF}_6]$ under argon. $E(\text{Cp}_2\text{Fe}^{+/0}) = 0.48$ V vs SCE.

bipyridine ligand. Complex **12** displays the most anodic $E_{1/2}^{\text{red}}$ value (-0.92 V vs. SCE) among the series due to the use of electron-deficient 2,2'-bipyrimidine ligand. For complexes supported by bis-carbene instead of diimine ligand, they display an irreversible oxidative wave at E_{pa} of 1.01–1.21 V vs. SCE but reduction wave was observed only for **14** which has a CF_3 group on the diacetyl ligand. From these electrochemical data, it is reasonable to conclude that the high-energy emission observed for **13–18** is due to their strongly destabilized LUMOs that are higher-lying by at least 1 eV as compared to those of **1–12**.

Photocatalysis: In literature, a number of Pt(II) complexes have been demonstrated as active catalysts for photoinduced C–C bond formation reactions and dehydrogenation

reactions.^[14b,16] Depending on the nature of excited states, the vacant axial coordination site of Pt(II) may allow for photochemical reaction with substrates via inner-sphere atom abstraction. A classic example is light-induced dehydrogenation of alcohols to give ketones and hydrogen by binuclear Pt(II) μ -pyrophosphito complex under oxidant-free and acceptorless conditions.^[17] We first examined photo-induced dehydrogenation of 1-phenylethanol by **8** in the absence of oxygen but no reaction was observed. Then, we examined the ability of the Pt(II) complexes developed in this work to sensitize the formation of singlet oxygen. By monitoring the emission intensity at 1270 nm in aerated chloroform solutions, the singlet oxygen quantum yields (Φ_{102}) of **4**, **8** and **18** were estimated to be 55%, 54% and 25%, respectively. The Φ_{102} of **4** and **8** are close to that of **8a** (the phenylacetylide counterpart complex of **8**; Φ_{102} = 62%). Then, complex **8** was selected as a representative example to study light-induced dehydrogenation of alcohols and alkenes under aerobic condition. Under light irradiation (410 nm LEDs) and in the presence of oxygen, complex **8** was found to catalyze the conversion of 1-phenylethanol to acetophenone in 96% yield after 12 hours (Table 3). Control experiments revealed that both oxygen and light are indispensable for the reaction (Table S5). 1-(4-Chlorophenyl) ethanol and 1-(3-methoxyphenyl) ethanol are also effective substrates for the reaction. Substrates with electron-withdrawing group (ester and trifluoromethyl; Table 3) also gave the product in good to excellent yields. We also examined the activity of **8a** in the light-induced aerobic oxidation of 1-phenylethanol. Under light irradiation (410 nm LEDs) and in the presence of **8a** and oxygen, only 4% of 1-phenylethanol was converted to acetophenone after 12 hours.

Table 3. Light-induced oxidation and dehydrogenation reactions catalyzed by complex **8**.^[a]

Yield (R) : 98 % (H)
99 % (3-OCH₃)
95 % (4-COOCH₃)
90 % (4-Cl)
88 % (4-CH₃)
80 % (4-CF₃)

Yield : 93 % ^[b]

Yield (R) : 95 % (H)
83 % (6-Cl)
72 % (5-Br)
68 % (6-NO₂)
66 % (5-CH₃)

[a] 0.1 mmol substrate, 1 mol% **8**, 2 mL solvent under O₂, 410 nm LED irradiation, 12 h. Yield determined by ¹H NMR spectroscopy using CH₂Br₂ as internal standard. [b] Yield determined by GC-MS.

Besides benzylic alcohols, complex **8** also catalyzed the light-induced oxidation of 1,4-cyclohexadiene to benzene in 93% yield under aerobic condition, but only trace amount of benzene was produced under N₂. Various indolines were converted to the corresponding indoles in good to excellent yields in the presence of **8** under oxygen and 410 nm LEDs irradiation (Table 3).

Biological studies: The luminescent, water-soluble Pt(II) diimine complex **11** bearing sulfonate groups was chosen for biological studies. Complex **11** displays a good water solubility at 20.2 g/L with lipophilicity parameter ($\log P_{o/w}$) of -0.95 . It is stable in aqueous buffer solution, RPMI-1640 cell culture medium and/or in the presence of biological reductant, glutathione, against hydrolysis or ligand exchange reaction, as revealed from mass spectrometric and UV/Vis spectroscopic analyses (Figures S26–S28). Confocal microscopy imaging revealed that the anionic, emissive **11** could be taken up by different cancer and normal cells and mainly co-localized with the red-emitting Lyso-Tracker (Pearson's colocalization coefficient (R) of 0.61 for NCI-H460, 0.53 for HCT116, 0.53 for MDA-MB-231 and 0.39 for CCD-19Lu) while it partially overlapped with Mito-Tracker (R of 0.46 for NCI-H460, 0.44 for HCT116, 0.29 for MDA-MB-231 and 0.12 for CCD-19Lu; Figure 14a–d). The emission spectra of the punctate staining in **11**-treated NCI-H460 lung cancer and CCD-19Lu normal lung fibroblast cells showed comparable emission maximum of 549 and 551 nm, respectively (Figure 14e). In **11**-treated HCT116 colorectal and MDA-MB-231 breast cancer cells, the emission bands were red-shifted with maximum at 564 and 565 nm, respectively. Cellular uptake of **11** was also confirmed by the time-dependent increase in cellular platinum content in different **11**-treated cells, as determined by ICP-MS (Figure 14f). From the *in vitro* anti-proliferative study on different cancer and normal cell lines, **11** treatment displayed relatively non-cytotoxic responses with IC₅₀ values in the range of 60.1 to greater than 100 μ M with respect to cisplatin (IC₅₀: 2.9–37.3 μ M) (Table 4).

The inhibition of *in vitro* angiogenesis by **11** was examined on a tube formation model of MS-1 murine endothelial cells cultured on Matrigel containing pro-angiogenic growth factors. In vehicle group, the cells interconnected with formation of branched network (Figure 15a). In contrast, treatment with **11** at non-cytotoxic concentration (50 μ M) for 4 h showed significant reduction of the tubular structures by 79% relative to vehicle control (Figure 15b), which is suggestive of the anti-angiogenic activity. Inhibition of tube formation was also observed in cells treated with the free sulfonated phenanthro-

Table 4. *In vitro* anti-proliferative activity (IC₅₀, μ M; 72 h) of **11** towards different human cancer and normal cell lines.^[a]

Compound	IC ₅₀ [μ M; 72 h]			
	NCI-H460	HCT116	MDA-MB-231	CCD-19Lu
11	99.4 ± 9.3	60.1 ± 8.4	67.3 ± 4.2	> 100
Cisplatin	2.9 ± 0.8	3.9 ± 0.6	19.3 ± 3.1	37.3 ± 4.8

[a] NCI-H460, Non-small cell lung carcinoma; HCT116, colorectal carcinoma; MDA-MB-231, triple-negative breast carcinoma; CCD-19Lu, normal lung fibroblast. Data are presented as mean \pm SD.

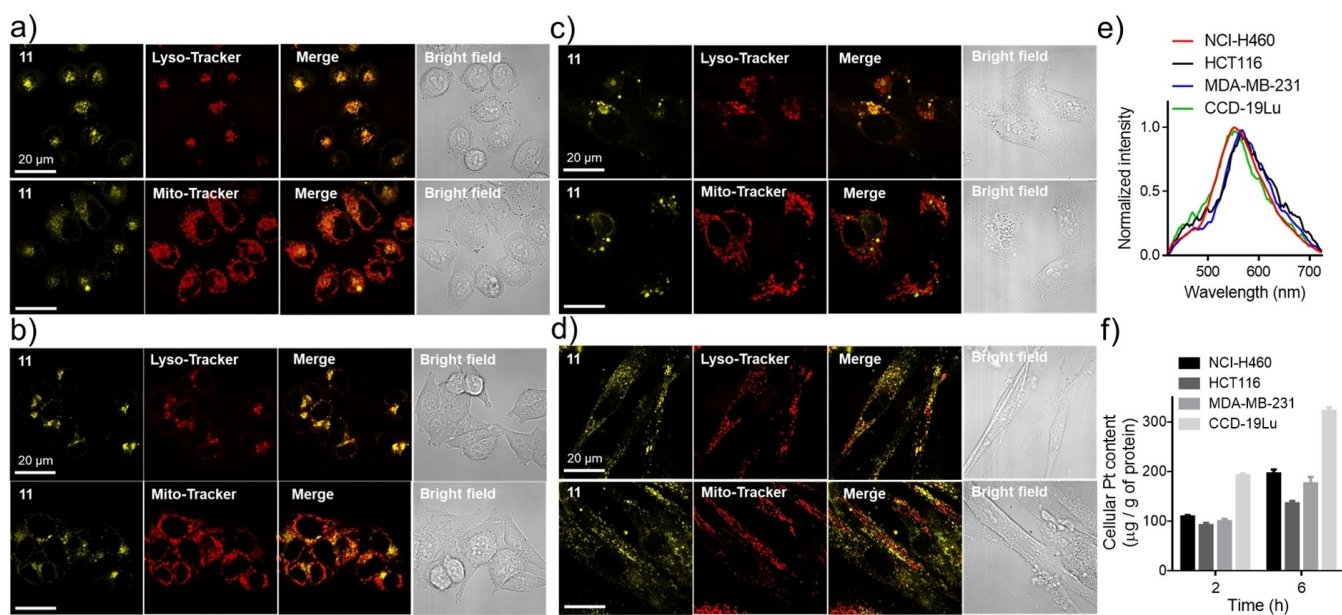


Figure 14. Confocal microscopy imaging of a) NCI-H460, b) HCT116, c) MDA-MB-231 or d) CCD-19Lu cells treated with complex 11 (20 µM; $\lambda_{\text{ex}} = 405$ nm, $\lambda_{\text{em}} = 430\text{--}620$ nm) for 2 h followed by co-incubation with Lyso- or Mito-Tracker Deep Red (50 nM; $\lambda_{\text{ex}} = 633$ nm, $\lambda_{\text{em}} = 650\text{--}740$ nm) for 15 min. The merged images of yellow and red channels, and the bright field were also shown. e) Emission spectra of 11-treated live cells recorded from confocal microscope using excitation at $\lambda_{\text{ex}} = 405$ nm. f) Cellular platinum content (µg Pt/g of protein) in different cells after treatment with 11 (20 µM) for 2 and 6 h.

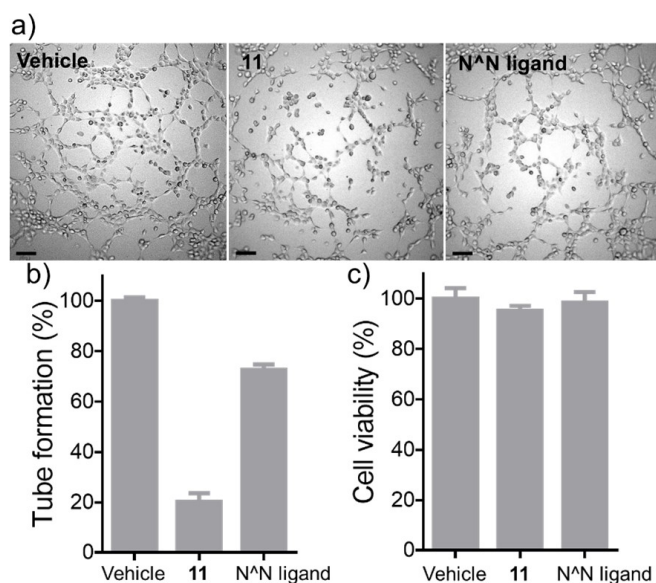


Figure 15. a) Tube formation assay of MS-1 endothelial cells treated with 11 or sulfonated diimine NN ligand (50 µM) for 4 h. Scale bar: 100 µm. Bar chart illustrates the percentage of b) inhibition of tube formation and c) cell viability as determined by CCK-8 assay.

line-based diimine ligand (sodium 4,4'-(1,10-phenanthroline-4,7-diyl)dibenzene-sulfonate, abbreviated as NN ligand in figure 15a and 15b) but the effect of which (27%) is not as good as that of 11 under the same experimental conditions. Such impairment of endothelial tube formation could possibly be attributed to the inhibition of biomolecular binding of the angiogenic growth factors to the associated cell membrane

receptors and signaling activation found in other sulfonated compounds with anti-angiogenic activities.^[18]

Discussion

In literature, arylacetylides have been extensively used to prepare luminescent Pt(II), Au(III) and Pd(II) complexes because these strong-field anionic carbon-donor ligands can effectively destabilize the $d\sigma^*$ ($d_{x^2-y^2}$) orbital and widen the $d-d$ field splitting, thus minimizing non-radiative decay and increasing emission quantum yield. Yet, in most cases, presumably due to easy access and preparation, these ligands are often used as a monodentate ligand. Since the thermal stability of metal complexes bearing bidentate or polydentate ligands would be improved compared to the ones bearing monodentate ligands as a result of chelate effect, we are interested in examining the use of one *cis*-chelating diacetylde ligand instead of two monodentate acetylde ligands to develop luminescent Pt(II) complexes. Pt(II) diimine complexes supported by *cis*-chelating diacetylde ligand have been reported but the photostability and photochemical properties of these complexes have not been examined. In this work, we prepared Pt(II) *cis*-chelating diacetylde complexes 1–18 and studied their properties.

The diacetylenes are constructed by stepwise Pd-catalyzed coupling and base deprotection. Coordination of Pt(II) with diacetylde ligand could be achieved with a catalytic amount of CuI and excess iPr_2NH with reference to reported procedure.^[2c,11] The X-ray crystal structures of 7, 8, 10 and 13 revealed that the coordination of these diacetylides to Pt(II) results in the 1,3-bridging phenyl being out-of-plane and forms a void within the diacetylde scaffold as shown in Figure 1. Although we have not

explored the properties or potential use associated with this interesting structure and the void, we conceive that if the central 1,3-bridging phenyl is replaced by 2,6-bridging pyridyl, this class of Pt(II) complexes may hold promise in sensing application such as toward metal ions via binding to pyridine and having π -interaction with the acetylene groups nearby.

Complexes 1–12 display absorption and emission spectral features similar to the Pt(II) diimine complexes with monodentate arylacetylides; they both show broad low-energy absorption bands and structureless emission bands associated with MLCT excited states. It is observed that for complexes with the same diimine ligand, the one with diacetylide having electron-withdrawing (CF_3) group shows the highest emission quantum yield and the one with electron-donating group (NPh_2) the lowest emission quantum yield (Φ : $2 > 1 > 3$; $5 > 4 > 6$; $9 > 8 > 10$). This is in accord with the trend observed in works of Eisenberg and Schanze in which the emission quantum yield of $[\text{Pt}(4,4'\text{-dtbbpy})(\text{C}\equiv\text{CC}_6\text{H}_4\text{X})_2]$ (where 4,4'-dtbbpy = 4,4'-di-*t*-butyl-2,2'-bipyridine; X = *para*-substituent) decreases with increasing electron-donating ability of X (In Eisenberg's work, Φ (X) = 14% (F), 11% (H), 7% (CH_3), 0.2% (OMe); in Schanze's work, Φ (X) = 20.7% (CF_3), 11.3% (H), 1.9% (OMe), 0.75% (NMe_2)).^[2a,b] For the Pt(II) diimine arylacetylide complexes in their studies, the relation between non-radiative decay rate constant and emission energy was found to obey the energy gap law.

When comparing the photophysical properties of **8** and **8a** (the phenylacetylide analogue of **8**), except for the red-shift in both absorption (11 nm) and emission (27 nm) for **8**, the emission quantum yield and lifetime of **8** are very close to the values for **8a**,^[2c] which suggests that the use of terphenyl diacetylide does not impose significant influence on radiative and non-radiative decay rate constants (for **8**, k_r and k_{nr} are $4.48 \times 10^5 \text{ s}^{-1}$ and $2.52 \times 10^5 \text{ s}^{-1}$, respectively; for **8a**, k_r and k_{nr} are $4.0 \times 10^5 \text{ s}^{-1}$ and $2.25 \times 10^5 \text{ s}^{-1}$, respectively). This is quite different from the finding in Castellano's study, in which the complex with the *cis*-chelating tolan-2,2'-diacetylide has its k_{nr} value ($9.8 \times 10^4 \text{ s}^{-1}$) reduced by $\sim 70\%$ compared to the k_{nr} of the phenylacetylide analogue ($3.6 \times 10^5 \text{ s}^{-1}$).^[6a] It is noted that in Castellano's study, the tolan-2,2'-diacetylide ligand is almost coplanar with the Pt(II) diimine scaffold, while in our study, the central 1,3-bridging phenyl of the diacetylide ligand is located above the Pt(II) coordination plane. The terphenyl diacetylide in our study may not be as rigid as the one in Castellano's study, leading to inefficient restriction of molecular motion and suppression of k_{nr} .

A notable difference in photostability was found between **8** and **8a**. Comparison of the ^1H NMR spectral change upon light irradiation of **8** and **8a** as shown in Figure S2 and S3, respectively, reveals that the use of chelating diacetylide renders the complex less prone to photo-degradation. The advantage of enhanced stability of **8** may be manifested in photocatalysis. As aforementioned, **8** catalyzed light-induced aerobic oxidation of 1-phenylethanol to acetophenone in 98% yield, while **8a** only gave the product in 4% yield. Since the Φ_{102} of **8** and **8a** differ by only $\sim 10\%$, the photocatalysis result suggests that the higher photo-stability of **8** could probably be the reason for the higher product yield compared to **8a**.

For the bis-NHC complexes **13–18**, they exhibit ^3IL phosphorescence localized on the diacetylide, similar to the phenylacetylide counterparts.^[12a] Importantly, the emission quantum yield of **16–18** having carbazole-appended diacetylide ligand are 23–28%, which are much higher than that of **13–15** with other substituents. Estimation of their k_r and k_{nr} reveals that the higher emission quantum yields of **16–18** are due to a remarkable reduction of k_{nr} from $2.3\text{--}3.6 \times 10^5 \text{ s}^{-1}$ (**13–15**) to $1.7\text{--}3.5 \times 10^4 \text{ s}^{-1}$ (i.e. reduced by one order of magnitude). The longer alkyl NHC side chain length of **13** (*n*-butyl) compared to that of **16–18** (methyl) may not be a major cause for the former's larger k_{nr} because varying the alkyl chain from methyl to *n*-butyl and *n*-hexyl does not result in a significant difference in k_{nr} in our previous study on $[\text{Pt}(\text{CN})(\text{bis-NHC})]^+$ (HCN = 2-arylpyridine).^[15b] A notable suppression of k_{nr} upon addition of carbazole on the ligand is also observed in tetradentate $[\text{Pt}(\text{OCCO})]$ complexes.^[14b,19] The reason why the presence of carbazole would lead to such improvement in emission properties in this work remains to be investigated by computational studies in the future.

Equipped with the two polar sulfonate groups on diimine ligand, the anionic complex **11** is soluble in aqueous media. A previous work showed that platinum(II) complex with sulfonated diimine and chlorido ligands displayed low anti-proliferative activity ($\text{IC}_{50} > 100 \mu\text{M}$) on HeLa cervical cancer cell line.^[20] Our work revealed that the incorporation of diacetylide ligand to platinum(II) complex with sulfonated diimine, as exemplified by **11**, confers good stability to the complex against ligand exchange reaction under physiological conditions. More importantly, the aqueous-soluble **11** is emissive that could be used for bio-imaging in different cancer cell lines. The emission λ_{max} (549–565 nm) of the dominant emission band in **11**-treated cells (Figure 14e) are close to the high-energy emission λ_{max} of **11** in water (570 nm, Table 1 and Figure 9) and that in RPMI-1640 medium (580 nm) (Figure S29). This could be attributed to the surrounding intracellular protein and/or extracellular serum that may assist the solvation of **11** under biological conditions, and hence resulting in the absence of the aggregate emission band at 706 nm.

In the literature, anionic sulfonated compounds have been reported to inhibit angiogenesis by interacting with the angiogenic growth factors (e.g., fibroblast growth factors, FGFs; vascular endothelial growth factor, VEGF) via hydrogen bonding and hydrophobic contacts, and hence hampering the functional interaction with the cell-surface protein receptors for angiogenic signaling.^[21] The effective suppression of the interconnection between the endothelial cells by treatment with **11** (Figure 15a) and the higher degree of inhibition of tube formation by **11** compared with that by the free sulfonated diimine ligand could be due to the possible biomolecular interaction of **11**, presumably governed by the distinct structural scaffold and decent lipophilicity, with the angiogenic growth factors resulting in the impairment of growth factor-receptor binding and activation.

Conclusions

In conclusion, we prepared two types of platinum(II) terphenyl diacetylide complexes with diimine and bis-*N*-heterocyclic carbene ligands. X-ray crystal structures of some of these compounds have revealed a curved conformation due to the steric strain of the *cis*-chelating diacetylide ligand. The photophysical and electrochemical properties of platinum(II) complexes **1–18** have been investigated. Complexes supported by diimine ligand exhibit ³MLCT emission while those supported by bis-NHC show ³IL emission. They display photoluminescence with quantum yields and lifetimes of up to 71% and 62 μs respectively in solution at room temperature. Compared with the previously reported bis-phenylacetylide complex **8a**, complex **8** shows enhanced photo-stability and photocatalytic activity in light-induced dehydrogenation of secondary alcohols under aerobic condition. The water soluble, anionic and relatively non-toxic complex **11** bearing polar sulfonates could be taken up by live cells with main localization in lysosomes and displays anti-angiogenic activity comparable to other sulfonate-containing angiogenesis inhibitors.

Experimental Section

All starting materials were purchased from commercial sources and used as received unless stated otherwise. The solvents used for synthesis were of analytical grade unless stated otherwise. The solvents used for photophysical measurements were of HPLC grade. ¹H, ¹³C, ¹⁹F, ¹⁹⁵Pt NMR spectra were recorded using a Bruker Avance 400 or 500 FT-NMR spectrometer. The high resolution mass spectra (HRMS) were obtained on a Thermo Scientific Q Exactive mass spectrometer, operated in electrospray ionization (ESI) mode, and coupled with Thermo Scientific Ultimate 3000 system. Elemental analyses (C, H and N) were performed on a Perkin-Elmer 240 C elemental analyzer. Steady-state emission spectra were recorded on a Horiba Fluorolog-3 spectrophotometer. UV/Vis absorption spectra were recorded on a Hewlett-Packard 8453 diode array spectrophotometer. The emission lifetime measurements were performed on a Quanta Ray GCR 150-10 pulsed Nd: YAG laser system. Φ values were measured relative to that of a solution of quinine sulfate in 0.5 M H₂SO₄ (Φ = 0.546) as a standard reference and calculated by: $\Phi_s = \Phi_r (B_s/B_r)(n_s/n_r)^2(D_s/D_r)$, where the subscripts s and r refer to sample and reference standard solutions, respectively, n is the refractive index of the solvents, D is the integrated intensity, and Φ is the luminescence quantum yield. The excitation intensity B was calculated by: $B = 1 - 10^{-AL}$, where A is the absorbance at the excitation wavelength and L is the optical path length (L = 1 cm in all cases). Errors for λ values (± 1 nm), τ (± 10%), Φ (± 10%) were estimated. Solutions for photophysical studies were degassed by using a high vacuum line in a two-compartment cell with five freeze-pump-thaw cycles. Φ₁₀₂ were estimated by taking the Φ₁₀₂ of tetraphenylporphyrin (H₂TPP) in air-saturated CHCl₃ to be 55%.^[22] The X-ray diffraction data were collected at 100 K on a Bruker D8 Venture single crystal X-ray diffractometer. CCDC 2094193 (**7**), 2094194 (**8**), 2094195 (**10**), and 2094196 (**13**) contain the supplementary crystallographic data for this paper. These data can be obtained free of charge from The Cambridge Crystallographic Data Centre. Cyclic voltammetry measurements were performed on a Princeton Applied Research Parstat potentiostat (PMC 1000) with a glassy carbon electrode (d = 2 mm) with a Pt counter electrode versus SCE reference electrode. The mass spectra for the stability study were recorded using Thermo Scientific TSQ Altis Triple

Quadrupole Mass Spectrometer. Light scattering measurements were conducted with ZetaView Nanoparticle Tracking Video Microscope PMX-120. Confocal microscopy imaging and the corresponding emission spectra in live cells were performed on a Carl Zeiss LSM 880 confocal laser scanning microscope. Cellular uptake and lipophilicity parameter of the platinum complex were determined in platinum content using Agilent 7700x inductively coupled plasma mass spectrometer. The absorbance for the NBB (Naphthol blue black dye; 620 nm) or CCK-8 (Cell counting kit-8; 450 nm) assay on determining the cell viability was measured by Thermal Scientific Varioskan LUX multiplate reader.

Syntheses and characterization

The compounds bpy and Pt(bpy)Cl₂ (bpy = 4,4'-bis(4-(trifluoromethyl)phenyl)-2,2'-bipyridine or 4,4'-bis(4-(*t*-butyl)phenyl)-2,2'-bipyridine) were prepared following literature methods.^[2c,11] The compounds 1,1'-methylenebis(3-butyl-1H-imidazol-3-ium) and Pt(bis-NHC)Cl₂ (bis-NHC = bis(3-butyl-2,3-dihydro-1H-imidazol-1-yl)methane or bis(3-methyl-2,3-dihydro-1H-imidazol-1-yl)methane) were prepared previously literature methods.^[12b] The precursor for 2,2'-diethynyl-1,1':3',1''-terphenyl (**L1**) was prepared following literature methods.^[23] 4,4'-bis(4-(*t*-butyl)phenyl)-2,2'-bipyrimidine were prepared following literature methods.^[24] Details of experiments are shown in the supporting information.

Complex 1: A mixture of Pt(bpy)Cl₂ (bpy = 4,4'-bis(4-(trifluoromethyl)phenyl)-2,2'-bipyridine) (50 mg, 0.07 mmol), *i*Pr₂NH (1 mL, 722 mg, 7.14 mmol), **L1** (78 mg, 0.14 mmol) and anhydrous CuI (1 mg, 0.007 mmol) in dry DMF (5 mL) was stirred at room temperature under dry N₂ for 24 h. The mixture was filtered and washed with diethyl ether. A red solid was obtained (50 mg, 78% yield). ¹H NMR (400 MHz, DMSO-*d*₆): δ = 9.51 (d, *J* = 5.8 Hz, 2H; bpy), 9.21 (s, 2H; bpy), 8.65 (s, 1H; Ph), 8.31 (d, *J* = 7.7 Hz, 5H; bpy and Ph), 8.02 (d, *J* = 8.3 Hz, 4H; Ph), 7.53 (dd, *J* = 15.0, 7.3 Hz, 4H; Ph), 7.29 (d, *J* = 5.9 Hz, 8H; Ph); ¹⁹F NMR (376 MHz, DMSO-*d*₆): δ = -61.2; IR (KBr): ν = 2112 cm⁻¹ (C≡C); HRMS (ESI): *m/z*: [M + H]⁺ calculated for C₄₆H₂₇N₂F₆Pt: 916.1721; found: 916.1721; Elemental analyses for C₄₆H₂₆F₆N₂Pt: C, 60.33; H, 2.86; N, 3.06. Found: C, 60.48; H, 2.97; N, 3.09.

Complex 2: The synthesis was similar to that of complex 1. A red solid was obtained (53 mg, 77%). ¹H NMR (400 MHz, DMSO-*d*₆): δ = 9.49 (d, *J* = 5.8 Hz, 2H; bpy), 9.21 (s, 2H; bpy), 8.83 (s, 1H; Ph), 8.31 (d, *J* = 7.6 Hz, 6H; bpy and Ph), 8.02 (d, *J* = 8.3 Hz, 4H; Ph), 7.58 (d, *J* = 7.8 Hz, 4H; Ph), 7.33 (m, 6H; Ph); ¹⁹F NMR (376 MHz, DMSO-*d*₆): δ = -60.8, -61.2; IR (KBr): ν = 2133 cm⁻¹ (C≡C); HRMS (ESI): *m/z*: [M + H]⁺ calculated for C₄₇H₂₆N₂F₉Pt: 984.1595; found: 984.1587; Elemental analyses (%) for C₄₇H₂₅F₉N₂Pt: C, 57.38; H, 2.56; N, 2.85. Found: C, 57.09; H, 2.51; N, 2.77.

Complex 3: The synthesis was similar to that of complex 1. A red solid was obtained (40 mg, 53%). ¹H NMR (400 MHz, DMSO-*d*₆): δ = 9.53 (d, *J* = 6.0 Hz, 2H; bpy), 9.23 (s, 2H; bpy), 8.44 (s, 1H; Ph), 8.32 (d, *J* = 8.1 Hz, 5H; bpy and Ph), 8.03 (d, *J* = 8.3 Hz, 4H; Ph), 7.54 (d, *J* = 7.5 Hz, 2H; Ph), 7.36–7.31 (m, 4H; Ph), 7.29–7.24 (m, 3H; Ph), 7.22–7.16 (m, 4H; Ph), 7.16–7.11 (m, 4H; Ph), 7.08–7.03 (m, 2H; Ph), 6.89 (s, 2H; Ph); ¹⁹F NMR (376 MHz, DMSO-*d*₆): δ = -61.2; IR (KBr): ν = 2116 cm⁻¹ (C≡C); HRMS (ESI): *m/z*: [M + H]⁺ calculated for C₅₈H₃₆N₃F₆Pt: 1083.2456; found: 1083.2437; Elemental analyses (%) for C₅₈H₃₅F₆N₃Pt: C, 64.32; H, 3.26; N, 3.88. Found: C, 64.46; H, 3.33; N, 3.92.

Complex 4: The synthesis was similar to that of complex 1. A yellow solid was obtained (55 mg, 85%). ¹H NMR (400 MHz, DMSO-*d*₆): δ = 9.42 (d, *J* = 5.9 Hz, 2H; bpy), 9.11 (s, 2H; bpy), 8.67 (s, 1H; Ph), 8.22 (d, *J* = 4.2 Hz, 2H; bpy), 8.05 (d, *J* = 8.4 Hz, 4H; Ph), 7.65 (d, *J* = 8.5 Hz, 4H; Ph), 7.56–7.50 (m, 4H; Ph), 7.30–7.26 (m, 7H; Ph) 1.36 (s, 18H;

$C(CH_3)_3$; IR (KBr): $\nu = 2109\text{ cm}^{-1}$ ($C \equiv C$); HRMS (ESI): m/z : $[M + H]^+$ calculated for $C_{52}H_{45}N_2Pt$: 892.3225; found: 892.3229; Elemental analyses (%) for $C_{52}H_{44}N_2Pt$: C, 70.02; H, 4.97; N, 3.14. Found: C, 70.16; H, 5.02; N, 3.17.

Complex 5: The synthesis was similar to that of complex 1. A yellow solid was obtained (52 mg, 74%). 1H NMR (400 MHz, DMSO- d_6): $\delta = 9.40$ (d, $J = 5.9$ Hz, 2H; bpy), 9.11 (s, 2H; bpy), 8.84 (s, 1H; Ph), 8.21 (d, $J = 5.7$ Hz, 2H; bpy), 8.04 (d, $J = 8.4$ Hz, 4H; Ph), 7.65 (d, $J = 8.4$ Hz, 4H; Ph), 7.58 (d, $J = 8.7$ Hz, 4H; Ph), 7.38–7.28 (m, 6H; Ph), 1.36 (s, 18H; $C(CH_3)_3$); ^{19}F NMR (376 MHz, DMSO- d_6): $\delta = -60.8$. IR (KBr): $\nu = 2134\text{ cm}^{-1}$ ($C \equiv C$); HRMS (ESI): m/z : $[M + H]^+$ calculated for $C_{53}H_{44}N_2F_3Pt$: 960.3099; found: 960.3099; Elemental analyses (%) for $C_{53}H_{43}F_3N_2Pt$: C, 66.31; H, 4.51; N, 2.92. Found: C, 66.28; H, 4.39; N, 2.88.

Complex 6: The synthesis was similar to that of complex 1. A yellow solid was obtained (42 mg, 55%). 1H NMR (400 MHz, DMSO- d_6): $\delta = 9.44$ (d, $J = 5.9$ Hz, 2H; bpy), 9.12 (s, 2H; bpy), 8.45 (s, 1H; Ph), 8.23 (d, $J = 5.9$ Hz, 2H; bpy), 8.06 (d, $J = 8.5$ Hz, 4H; Ph), 7.66 (d, $J = 8.5$ Hz, 4H; Ph), 7.54 (d, $J = 7.6$ Hz, 2H; Ph), 7.33 (t, $J = 7.9$ Hz, 4H; Ph), 7.26 (t, $J = 7.5$ Hz, 2H; Ph), 7.21–7.11 (m, 8H; Ph), 7.06 (t, $J = 7.3$ Hz, 2H; Ph), 6.89 (d, $J = 1.4$ Hz, 2H; Ph), 1.37 (s, 18H; $C(CH_3)_3$); IR (KBr): $\nu = 2134\text{ cm}^{-1}$ ($C \equiv C$); HRMS (ESI): m/z : $[M + H]^+$ calculated for $C_{64}H_{54}N_3Pt$: 1059.3960; found: 1059.3951; Elemental analyses (%) for $C_{64}H_{53}N_3Pt$: C, 72.57; H, 5.04; N, 3.97. Found: C, 72.22; H, 4.85; N, 4.01.

Complex 7: A mixture of $Pt(bpy)Cl_2$ (bpy = 4,4'-bis(2,6-dimethylphenyl)-2,2'-bipyridine) (50 mg, 0.08 mmol), iPr_2NH (1 mL, 722 mg, 7.14 mmol), L1 (40 mg, 0.12 mmol) and CuI (1 mg, 0.007 mmol) in dry DCM (5 mL) was stirred at room temperature under dry N_2 for 24 h. After removing dichloromethane under reduced pressure, the residue purified by column chromatography on silica gel with petroleum ether/dichloromethane (3:1) as eluent to afford a red solid (40 mg, 56% yield). 1H NMR (500 MHz, $CDCl_3$): $\delta = 9.84$ (d, $J = 5.6$ Hz, 2H; bpy), 8.65 (t, $J = 1.6$ Hz, 1H; Ph), 7.76 (t, $J = 1.0$ Hz, 2H; bpy), 7.40 (m, 3H; bpy and Ph), 7.27 (dd, $J = 1.8, 1.7$ Hz, 2H; Ph), 7.22 (t, $J = 7.6$ Hz, 2H; Ph), 7.12 (s, 4H; Ph), 7.00 (d, $J = 11.35$ Hz, 4H; Ph), 2.69 (s, 6H; CH_3), 2.32 (s, 6H; CH_3), 2.08 (s, 6H; CH_3), 1.99 (s, 6H; CH_3); ^{13}C NMR (126 MHz, $CDCl_3$): $\delta = 156.5$ (bpy), 152.7 (bpy), 152.2 (bpy), 145.3 (bpy), 141.5 (bpy), 139.7 (Ph), 137.3 (Ph), 134.7 (Ph), 134.2 (Ph), 129.1 (Ph), 128.5 (Ph), 128.5 (Ph), 128.1 (Ph), 127.9 (Ph), 127.8 (Ph), 123.2 (Ph), 122.8 (Ph), 100.2 (Pt– $C \equiv C$), 89.4 (Pt– $C \equiv C$), 22.3 (CH_3), 21.5 (CH_3), 20.9 (CH_3); ^{195}Pt NMR (107 MHz, $CDCl_3$, 25 °C): $\delta = -3583.4$; IR (KBr): $\nu = 2115\text{ cm}^{-1}$ ($C \equiv C$); HRMS (ESI): m/z : $[M + H]^+$ calculated for $C_{52}H_{45}N_2Pt$: 892.3225; found: 892.3230; Elemental analyses (%) for $C_{52}H_{44}N_2Pt$: C, 70.02; H, 4.97; N, 3.14. Found: C, 69.66; H, 4.81; N, 2.88.

Complex 8: The synthesis was similar to that of complex 7. An orange solid was obtained (50 mg, 65%). 1H NMR (400 MHz, CD_2Cl_2): $\delta = 9.32$ (s, 2H; bpy), 8.86 (s, 1H; Ph), 7.84 (s, 4H; bpy), 7.59 (d, $J = 7.2$ Hz, 2H; Ph), 7.33 (d, $J = 7.4$ Hz, 2H; Ph), 7.18–7.27 (m, 6H; Ph), 6.96 (s, 2H; Ph), 2.50 (s, 6H; CH_3), 2.31 (s, 3 H; CH_3), 2.17 (s, 6H; CH_3); IR (KBr): $\nu = 2130\text{ cm}^{-1}$ ($C \equiv C$); HRMS (ESI): m/z : $[M + H]^+$ calculated for $C_{43}H_{35}N_2Pt$: 774.2443, found: 774.2430; Elemental analyses (%) for $C_{43}H_{34}N_2Pt$: C, 66.74; H, 4.43; N, 3.62. Found: C, 66.13; H, 4.16; N, 3.43.

Complex 9: The synthesis was similar to that of complex 7. A yellow solid was obtained (42 mg, 53%). 1H NMR (400 MHz, CD_2Cl_2): $\delta = 9.35$ (s, 2H; bpy), 8.72 (s, 1H; Ph), 7.84–7.91 (m, 6H; bpy and Ph), 7.72 (d, $J = 8.1$ Hz, 2H; Ph), 7.59–7.62 (m, 4H; Ph), 7.39 (d, $J = 7.4$ Hz, 2H; Ph), 7.25–7.32 (m, 4H; Ph), 2.51 (s, 6 H; CH_3); ^{19}F NMR (376 MHz, CD_2Cl_2): $\delta = -62.6$; IR (KBr): $\nu = 2119\text{ cm}^{-1}$ ($C \equiv C$); HRMS (ESI): m/z : $[M + H]^+$ calculated for $C_{41}H_{28}N_2F_3Pt$: 800.1847, found: 800.1816; Elemental analyses (%) for $C_{41}H_{27}F_3N_2Pt$: C, 61.57; H, 3.40; N, 3.50. Found: C, 61.41; H, 3.35; N, 3.47.

Complex 10: The synthesis was similar to that of complex 7. An orange-red solid was obtained (65 mg, 72%). 1H NMR (400 MHz, CD_2Cl_2): $\delta = 9.37$ (s, 2H; bpy), 8.64 (s, 2H; bpy and Ph), 7.84–7.90 (m, 4H; bpy), 7.61 (t, $J = 7.8$ Hz, 4H; Ph), 7.54 (d, $J = 1.4$ Hz, 2H; Ph), 7.38–7.40 (m, 3H; Ph), 7.23–7.30 (m, 7H; Ph), 7.13 (d, $J = 8.3$ Hz, 5H; Ph), 7.03 (t, $J = 7.3$ Hz, 2H; Ph), 2.52 (s, 6H; CH_3); IR (KBr): $\nu = 2114\text{ cm}^{-1}$ ($C \equiv C$); HRMS (ESI): m/z : $[M + H]^+$ calculated for $C_{52}H_{38}N_3Pt$: 899.2708, found: 899.2675; Elemental analyses (%) for $C_{52}H_{37}N_3Pt$: C, 69.48; H, 4.15; N, 4.67. Found: C, 69.29; H, 4.13; N, 4.53.

Complex 11: The synthesis was similar to modified that of complex 1. A red solid was obtained (30 mg, 50%). 1H NMR (500 MHz, DMSO- d_6): $\delta = 9.76$ (s, 2H; phen), 8.72 (s, 1H; Ph), 8.18 (d, $J = 5.0$ Hz, 2H; phen), 8.07 (s, 2H; phen), 7.92 (s, 2H; Ph), 7.85 (d, $J = 7.5$ Hz, 2H; Ph), 7.69 (d, $J = 7.4$ Hz, 2H; Ph), 7.63 (d, $J = 6.8$ Hz, 4H; Ph), 7.57–7.51 (m, 1H; Ph), 7.35–7.24 (m, 8H; Ph); IR (KBr): $\nu = 2136\text{ cm}^{-1}$ ($C \equiv C$); HRMS (ESI): m/z : $[M - 2Na]^{2-}$ calculated for $C_{46}H_{26}N_2O_6PtS_2$: 480.5445, found: 480.5454; Elemental analyses (%) for $C_{46}H_{26}N_2Na_2O_6PtS_2$: C, 54.82; H, 2.60; N, 2.78. Found: C, 54.61; H, 2.55; N, 2.75.

Complex 12: The synthesis was similar to that of complex 7. A red solid was obtained (46 mg, 74%). 1H NMR (500 MHz, $CDCl_3$): $\delta = 9.55$ (d, $J = 5.9$ Hz, 2H; bipyrimidine), 8.44 (s, 1H; Ph), 8.17 (d, $J = 8.4$ Hz, 4H; bipyrimidine and Ph), 7.79 (d, $J = 6.0$ Hz, 2H; Ph), 7.59–7.54 (m, 2H; Ph), 7.53 (s, 2H; Ph), 7.52 (s, 2H; Ph), 7.42 (s, 1H; Ph), 7.25 (d, $J = 1.7$ Hz, 4H; Ph), 7.24–7.19 (m, 4H; Ph), 1.39 (s, 18H; $C(CH_3)_3$); ^{13}C NMR (126 MHz, $CDCl_3$): $\delta = 164.7$ (bipyrimidine), 161.9 (bipyrimidine), 157.8 (bipyrimidine), 156.7 (bipyrimidine), 144.8 (Ph), 140.9 (Ph), 133.6 (Ph), 133.1 (Ph), 132.0 (Ph), 130.2 (Ph), 128.1 (Ph), 128.0 (Ph), 127.9 (Ph), 126.5 (Ph), 126.5 (Ph), 125.9 (Ph), 125.6 (Ph), 118.5 (Ph), 101.7 (Pt– $C \equiv C$), 85.5 (Pt– $C \equiv C$), 35.3 ($C(CH_3)_3$), 31.2 ($C(CH_3)_3$); IR (KBr): $\nu = 2110\text{ cm}^{-1}$ ($C \equiv C$); HRMS (ESI): m/z : $[M + H]^+$ calculated for $C_{50}H_{43}N_4Pt$: 894.3130; found: 894.3118; Elemental analyses (%) for $C_{50}H_{42}N_4Pt$: C, 67.18; H, 4.74; N, 6.27. Found: C, 66.76; H, 4.76; N, 6.01.

Complex 13: A mixture of $Pt(bis-NHC)Cl_2$ (bis-NHC = bis(3-butyl-2,3-dihydro-1H-imidazol-1-yl)methane) (50 mg, 0.09 mmol), iPr_2NH (1 mL, 722 mg, 7.14 mmol), L1 (50 mg, 0.18 mmol) and anhydrous CuI (1 mg, 0.007 mmol) in dry DMF (5 mL) was stirred at room temperature under dry N_2 for 24 h. The solvent was removed under reduced pressure. The residue was purified by column chromatography with hexane/ CH_2Cl_2 (5:1) to afford a pale-yellow solid (58 mg, 83% yield). 1H NMR (500 MHz, $CDCl_3$): $\delta = 9.02$ (s, 1H; Ph), 7.47 (d, $J = 7.2$ Hz, 1H; Ph), 7.35 (d, $J = 6.6$ Hz, 4H; Ph), 7.28 (s, 2H; Ph), 7.16 (s, 4H; Ph), 6.52 (d, $J = 13.6$ Hz, 5H; carbene and $-CHH-$), 5.07 (s, 2H; $CHHCH_2CH_2CH_3$), 4.49 (s, 1H; $-CHH-$), 4.10 (s, 2H; $CHHCH_2CH_2CH_3$), 1.70 (m, 4H; $CH_2CH_2CH_2CH_3$), 1.27 (m, 4H; $CH_2CH_2CH_2CH_3$), 0.86 (t, $J = 6.9$ Hz, 6H; $CH_2CH_2CH_2CH_3$); ^{13}C NMR (126 MHz, $CDCl_3$): $\delta = 167.0$ (C=Pt), 143.1 (Ph), 141.9 (Ph), 135.0 (Ph), 132.8 (Ph), 130.1 (Ph), 128.2 (Ph), 127.6 (Ph), 127.0 (Ph), 126.8 (Ph), 125.2 (Ph), 120.2 (carbene), 119.2 (carbene), 107.3 (Pt– $C \equiv C$), 106.8 (Pt– $C \equiv C$), 65.2 ($-CH_2-$), 50.3 ($CH_2CH_2CH_2CH_3$), 33.4 ($CH_2CH_2CH_2CH_3$), 19.9 ($CH_2CH_2CH_2CH_3$), 14.0 ($CH_2CH_2CH_2CH_3$); ^{195}Pt NMR (107 MHz, $CDCl_3$, 25 °C): $\delta = -4314.0$; IR (KBr): $\nu = 2112\text{ cm}^{-1}$ ($C \equiv C$); HRMS (ESI): m/z : $[M + H]^+$ calculated for $C_{37}H_{37}N_4Pt$: 732.2661; found: 732.2672; Elemental analyses (%) for $C_{37}H_{36}N_4Pt$: C, 60.73; H, 4.96; N, 7.66. Found: C, 60.58; H, 4.86; N, 7.52.

Complex 14: The synthesis was similar to that of complex 13. A pale-yellow solid was obtained (65 mg, 86% yield). 1H NMR (400 MHz, $CDCl_3$): $\delta = 9.07$ (s, 1H; Ph), 7.50 (s, 2H; Ph), 7.38 (dd, $J = 6.1, 2.7$ Hz, 2H; Ph), 7.26 (t, $J = 3.1$ Hz, 2H; Ph), 7.22–7.14 (m, 4H; Ph), 6.68 (d, $J = 39.8$ Hz, 4H; carbene), 5.91 (d, $J = 12.3$ Hz, 1H; $-CHH-$), 5.37 (s, 1H; $-CHH-$), 4.96 (s, 2H; $CHHCH_2CH_2CH_3$), 4.26 (s, 2H; $CHHCH_2CH_2CH_3$), 1.79 (d, $J = 9.4$ Hz, 4H; $CH_2CH_2CH_2CH_3$), 1.34 (s, 4H; $CH_2CH_2CH_2CH_3$), 0.90 (t, $J = 7.3$ Hz, 6H; $CH_2CH_2CH_2CH_3$); ^{13}C NMR (126 MHz, $CDCl_3$): $\delta = 167.1$ (C=Pt), 142.3 (Ph), 142.2 (Ph), 137.8 (Ph),

132.6 (Ph), 130.3 (q, $^2J_{C-F} = 32.0$ Hz, Ph), 130.0 (Ph), 127.3 (Ph), 126.7 (Ph), 125.6 (Ph), 124.5 (q, $^1J_{C-F} = 272.9$ Hz, CF_3), 124.2 (q, $^3J_{C-F} = 3.8$ Hz, Ph), 121.3 (carbene), 119.5 (carbene), 107.5 (Pt–C≡C), 106.9 (Pt–C≡C), 63.8 (–CH₂–), 50.5 (CH₂CH₂CH₂CH₃), 33.3 (CH₂CH₂CH₂CH₃), 19.9 (CH₂CH₂CH₂CH₃), 13.9 (CH₂CH₂CH₂CH₃); ^{19}F NMR (376 MHz, $CDCl_3$): $\delta = -62.1$; IR (KBr): $\nu = 2110$ cm⁻¹ (C≡C); HRMS (ESI): m/z: [M+H]⁺ calculated for C₃₈H₃₆N₄F₃Pt: 800.2534; found: 800.2546; Elemental analyses (%) for C₃₈H₃₅F₃N₄Pt: C, 57.07; H, 4.41; N, 7.01. Found: C, 56.96; H, 4.58; N, 7.02.

Complex 15: The synthesis was similar to that of complex 13. A pale-yellow solid was obtained (30 mg, 66% yield). 1H NMR (400 MHz, DMSO-d₆): $\delta = 7.54$ (s, 2H; Ph), 7.39–7.31 (m, 10H; Ph), 7.25–7.19 (m, 7H; Ph), 7.11–7.05 (m, 4H; Ph and carbene), 6.86 (s, 2H; Ph), 6.02 (br, 2H; –CH₂–), 4.02 (s, 6H; CH₃); IR (KBr): $\nu = 2109$ cm⁻¹ (C≡C); HRMS (ESI): m/z: [M+H]⁺ calculated for C₄₃H₃₄N₅Pt: 815.2456; found: 815.2434; Elemental analyses (%) for C₄₃H₃₃N₅Pt: C, 63.38; H, 4.08; N, 8.59. Found: C, 63.08; H, 3.85; N, 8.47.

Complex 16: A mixture of **L8** (49 mg, 0.08 mmol), *i*Pr₂NH (1 mL, 722 mg, 7.14 mmol), Pt(COD)Cl₂ (31 mg, 0.08 mmol) and anhydrous CuI (0.2 mg, 0.0008 mmol) in dry DMF (5 mL) was stirred at room temperature under dry N₂ for 24 h. Then 1,1'-methylenebis(1,3-dihydro-3-methyl-2H-imidazol-2-ylidene) (27 mg, 0.08 mmol) and NaOAc (13 mg, 0.16 mmol) were added into the mixture. The mixture was heated at 70 °C for 12 hours and then cooled to room temperature. After evaporation to dryness, the crude product was purified by column chromatography with a CH₂Cl₂:CH₃CN (20:1) mixture to afford the target compound as a white solid (45 mg, 57% yield). 1H NMR (500 MHz, $CDCl_3$): 1H NMR (500 MHz, $CDCl_3$) δ 9.18 (s, 1H; Ph), 8.12 (d, $J = 7.7$ Hz, 4H; Ph), 7.64 (d, $J = 8.2$ Hz, 2H; Ph), 7.47 (d, $J = 8.0$ Hz, 5H; Ph), 7.39 (dd, $J = 15.3, 7.9$ Hz, 7H; Ph), 7.27 (s, 7H; Ph), 6.86 (d, $J = 25.9$ Hz, 4H; carbene), 5.29 (s, 2H; –CH₂–), 4.22 (s, 6H; CH₃); IR (KBr): $\nu = 2110$ cm⁻¹ (C≡C); HRMS (ESI): m/z: [M+H]⁺ calculated for C₅₅H₃₉N₆Pt: 978.2878; found: 978.2873; Elemental analyses (%) for C₅₅H₃₈N₆Pt: C, 67.54; H, 3.92; N, 8.59. Found: C, 67.27; H, 3.81; N, 8.55.

Complex 17: The synthesis was similar to that of complex 16. A white solid was obtained (46 mg, 56% yield). 1H NMR (500 MHz, $CDCl_3$) δ 9.20 (s, 1H; Ph), 8.13 (d, $J = 7.7$ Hz, 4H; Ph), 7.62 (d, $J = 8.1$ Hz, 2H; Ph), 7.51 (d, $J = 1.8$ Hz, 2H; Ph), 7.45 (d, $J = 8.2$ Hz, 4H; Ph), 7.40 (dd, $J = 13.2, 5.6$ Hz, 5H; Ph), 7.37–7.33 (m, 4H; Ph), 7.28 (s, 4H; Ph), 6.82 (d, $J = 1.3$ Hz, 2H; carbene), 6.64 (s, 2H; carbene), 5.25 (d, $J = 7.2$ Hz, 2H; –CH₂CH₂–), 4.15 (s, 6H; CH₃), 4.02 (d, $J = 7.3$ Hz, 2H; –CH₂CH₂–); IR (KBr): $\nu = 2112$ cm⁻¹ (C≡C); HRMS (ESI): m/z: [M+H]⁺ calculated for C₅₆H₄₁N₆Pt: 992.3035; found: 992.3027; Elemental analyses (%) for C₅₆H₄₀N₆Pt: C, 67.80; H, 4.06; N, 8.47. Found: C, 67.26; H, 4.17; N, 8.51.

Complex 18: The synthesis was similar to that of complex 16. A white solid was obtained (40 mg, 40% yield). 1H NMR (500 MHz, $CDCl_3$) δ 9.15 (s, 1H; Ph), 8.11 (d, $J = 7.7$ Hz, 4H; Ph), 7.61 (d, $J = 8.2$ Hz, 2H; Ph), 7.46 (d, $J = 2.1$ Hz, 2H; Ph), 7.39 (dt, $J = 23.7, 8.4$ Hz, 9H; Ph), 7.33 (s, 2H; Ph), 7.30–7.27 (m, 2H; Ph), 7.24 (d, $J = 7.1$ Hz, 3H; Ph), 6.81 (d, $J = 1.2$ Hz, 2H; carbene), 6.73 (d, $J = 1.6$ Hz, 2H; carbene), 5.09–4.94 (m, 2H; –CH₂CH₂CH₂–), 4.05 (s, 6H; CH₃), 3.99 (dd, $J = 14.5, 6.5$ Hz, 2H; –CH₂CH₂CH₂–), 2.34 (dd, $J = 15.3, 7.1$ Hz, 1H; –CH₂CHHCH₂–), 1.69 (d, $J = 15.7$ Hz, 1H; –CH₂CHHCH₂–); IR (KBr): $\nu = 2109$ cm⁻¹ (C≡C); HRMS (ESI): m/z: [M+H]⁺ calculated for C₅₇H₄₃N₆Pt: 1006.3191; found: 1006.3187; Elemental analyses (%) for C₅₇H₄₂N₆Pt: C, 68.05; H, 4.21; N, 8.35. Found: C, 67.65; H, 4.20; N, 8.31.

Acknowledgements

This work was supported by the Guangdong Major Project of Basic and Applied Basic Research (2019B030302009), the Science Technology and Innovation Commission of Shenzhen Municipality (JCYJ20180508162429786) and the Laboratory for Synthetic Chemistry and Chemical Biology under the Health@InnoHK Program launched by Innovation and Technology Commission. We thank the Southern University of Science and Technology for financial support. We also thank Prof. D. L. Phillips, Dr. L. Du and Miss X. Bai for conducting fs-ta spectroscopic measurements. Dr. K.-H. Low is thanked for the help with the construction of Hirshfeld surfaces.

Conflict of Interest

The authors declare no conflict of interest.

Keywords: luminescence · platinum · diimine · diacetylide · bis-N-Heterocyclic carbene

- [1] C.-W. Chan, L.-K. Cheng, C.-M. Che, *Coord. Chem. Rev.* **1994**, *132*, 87–97.
- [2] a) M. Hissler, W. B. Connick, D. K. Geiger, J. E. McGarrah, D. Lipa, R. J. Lachicotte, R. Eisenberg, *Inorg. Chem.* **2000**, *39*, 447–457; b) C. E. Whittle, J. A. Weinstein, M. W. George, K. S. Schanze, *Inorg. Chem.* **2001**, *40*, 4053–4062; c) S.-C. Chan, M. C. W. Chan, Y. Wang, C.-M. Che, K.-K. Cheung, N. Zhu, *Chem. Eur. J.* **2001**, *7*, 4180–4190; d) I. E. Pomestchenko, C. R. Luman, M. Hissler, R. Ziessel, F. N. Castellano, *Inorg. Chem.* **2003**, *42*, 1394–1396; e) Y. Kang, J. Lee, D. Song, S. Wang, *Dalton Trans.* **2003**, 3493–3499.
- [3] a) F. Guo, W. Sun, Y. Liu, K. Schanze, *Inorg. Chem.* **2005**, *44*, 4055–4065; b) H. Sun, H. Guo, W. Wu, X. Liu, J. Zhao, *Dalton Trans.* **2011**, *40*, 7834–7841.
- [4] a) V. W.-W. Yam, R. P.-L. Tang, K. M.-C. Wong, K.-K. Cheung, *Organometallics* **2001**, *20*, 4476–4482; b) Q.-Z. Yang, L.-Z. Wu, Z.-X. Wu, L.-P. Zhang, C.-H. Tung, *Inorg. Chem.* **2002**, *41*, 5653–5655; c) W. Lu, B.-X. Mi, M. C. W. Chan, Z. Hui, C.-M. Che, N. Zhu, S.-T. Lee, *J. Am. Chem. Soc.* **2004**, *126*, 4958–4971; d) D. Zhang, L.-Z. Wu, L. Zhou, X. Han, Q.-Z. Yang, L.-P. Zhang, C.-H. Tung, *J. Am. Chem. Soc.* **2004**, *126*, 3440–3441; e) P. Du, J. Schneider, P. Jarosz, R. Eisenberg, *J. Am. Chem. Soc.* **2006**, *128*, 7726–7727; f) P. Du, R. Eisenberg, *Chem. Sci.* **2010**, *1*, 502–506.
- [5] Selected reviews: a) K. M.-C. Wong, V. W.-W. Yam, *Acc. Chem. Res.* **2011**, *44*, 424–434; b) Z. Gao, Y. Han, Z. Gao, F. Wang, *Acc. Chem. Res.* **2018**, *51*, 2719–2729; c) W. Yang, J. Zhao, *Eur. J. Inorg. Chem.* **2016**, 5283–5299; d) A. Haque, L. Xu, R. A. Al-Balushi, M. K. Al-Suti, R. Ilmi, Z. Guo, M. S. Khan, W.-Y. Wong, P. R. Raithby, *Chem. Soc. Rev.* **2019**, *48*, 5547–5563.
- [6] a) F. Hua, S. Kinayyigit, J. R. Cable, F. N. Castellano, *Inorg. Chem.* **2006**, *45*, 4304–4306; b) Y. Fan, D. Zhao, *ACS Appl. Mater. Interfaces* **2015**, *7*, 6162–6171; c) Y. Ai, M. Ng, E. Y.-H. Hong, A. K.-W. Chan, Z.-W. Wei, Y. Li, V. W.-W. Yam, *Chem. Eur. J.* **2018**, *24*, 11611–11618.
- [7] a) F. Hua, S. Kinayyigit, A. A. Rachford, E. A. Shikhova, S. Goeb, J. R. Cable, C. J. Adams, K. Kirschbaum, A. A. Pinkerton, F. N. Castellano, *Inorg. Chem.* **2007**, *46*, 8771–8783; b) Y. Cao, M. O. Wolf, B. O. Patrick, *Inorg. Chem.* **2016**, *55*, 8985–8993.
- [8] a) M.-X. Zhu, W. Lu, N. Zhu, C.-M. Che, *Chem. Eur. J.* **2008**, *14*, 9736–9746; b) Y. Cao, M. O. Wolf, B. O. Patrick, *Inorg. Chem.* **2013**, *52*, 5636–5638; c) Y. Ai, M. H.-Y. Chan, A. K.-W. Chan, M. Ng, Y. Li, V. W.-W. Yam, *Proc. Natl. Acad. Sci. USA* **2019**, *116*, 13856–13861.
- [9] J. Lin, C. Zou, X. Zhang, Q. Gao, S. Suo, Q. Zhuo, X. Chang, M. Xie, W. Lu, *Dalton Trans.* **2019**, *48*, 10417–10421.
- [10] a) L. A. Büldt, X. Guo, A. Prescimone, O. S. Wenger, *Angew. Chem. Int. Ed.* **2016**, *55*, 11247–11250; *Angew. Chem.* **2016**, *128*, 11413–11417; b) L. A. Büldt, C. B. Larsen, O. S. Wenger, *Chem. Eur. J.* **2017**, *23*, 8577–8580;

- c) L. A. Büldt, X. Guo, R. Vogel, A. Prescimone, O. S. Wenger, *J. Am. Chem. Soc.* **2017**, *139*, 985–992.
- [11] S. L. James, M. Younus, P. R. Raithby, J. Lewis, *J. Organomet. Chem.* **1997**, *543*, 233–235.
- [12] a) Y. Zhang, J. A. Garg, C. Michelin, T. Fox, O. Blacque, K. Venkatesan, *Inorg. Chem.* **2011**, *50*, 1220–1228; b) Y. Zhang, J. Clavadetscher, M. Bachmann, O. Blacque, K. Venkatesan, *Inorg. Chem.* **2014**, *53*, 756–771.
- [13] a) M. J. Turner, J. J. McKinnon, S. K. Wolff, D. J. Grimwood, P. R. Spackman, D. Jayatilaka, M. A. Spackman, *CrystalExplorer17* (2017), University of Western Australia; b) M. A. Spackman, D. Jayatilaka, *CrystEngComm* **2009**, *11*, 19–32.
- [14] a) G. Cheng, P.-K. Chow, S. C. F. Kui, C.-C. Kwok, C.-M. Che, *Adv. Mater.* **2013**, *25*, 6765–6770; b) K. Li, Q. Y. Wan, C. Yang, X.-Y. Chang, K.-H. Low, C.-M. Che, *Angew. Chem. Int. Ed.* **2018**, *57*, 14129–14133; *Angew. Chem.* **2018**, *130*, 14325–14329.
- [15] a) H. Uesugi, T. Tsukuda, K. Takao, T. Tsubomura, *Dalton Trans.* **2013**, *42*, 7396–7403; b) T. Zou, C.-N. Lok, Y. M. E. Fung, C.-M. Che, *Chem. Commun.* **2013**, *49*, 5423–5425.
- [16] a) J.-J. Zhong, C. Yang, X.-Y. Chang, C. Zou, W. Lu, C.-M. Che, *Chem. Commun.* **2017**, *53*, 8948–8951; b) Z. Li, Y. Han, Z. Gao, T. Fu, F. Wang, *Mater. Chem. Front.* **2018**, *2*, 76–80; c) C. Y. Sun, W.-P. To, F.-F. Hung, X.-L. Wang, Z.-M. Su, C.-M. Che, *Chem. Sci.* **2018**, *9*, 2357–2364; d) A. M. Ranieri, L. K. Burt, S. Stagni, S. Zacchini, B. W. Skelton, M. I. Ogden, A. C. Bissember, M. Massi, *Organometallics* **2019**, *38*, 1108–1117; e) P. Domingo-Legarda, A. Casado-Sánchez, L. Marzo, J. Alemán, S. Cabrera, *Inorg. Chem.* **2020**, *59*, 13845–13857; f) H. Cheng, T.-L. Lam, Y. Liu, Z. Tang, C.-M. Che, *Angew. Chem. Int. Ed.* **2021**, *60*, 1383–1389; *Angew. Chem.* **2021**, *133*, 1403–1409.
- [17] J.-J. Zhong, W.-P. To, Y. G. Liu, W. Lu, C.-M. Che, *Chem. Sci.* **2019**, *10*, 4883–4889.
- [18] a) S. B. S. Takano, S. Gately, M. E. Neville, W. F. Herblin, J. L. Gross, H. Engelhard, M. Perricone, K. Eidsvoog, *Cancer Res.* **1994**, *54*, 2654–2660; b) M. Presta, D. Leali, H. Stabile, R. Ronca, M. Camozzi, L. Coco, E. Moroni, S. Liekens, M. Rusnati, *Curr. Pharm. Des.* **2003**, *9*, 553–566.
- [19] K. Li, X. Guan, C.-W. Ma, W. Lu, Y. Chen, C.-M. Che, *Chem. Commun.* **2011**, *47*, 9075–9077.
- [20] S. A. De Pascali, D. Migoni, P. Papadia, A. Muscella, S. Marsigliante, A. Ciccicarese, F. P. Fanizzi, *Dalton Trans.* **2006**, 5077–5087.
- [21] a) C. Fernández-Tornero, R. M. Lozano, M. Redondo-Horcajo, A. M. Gómez, J. C. López, E. Quesada, C. Uriel, S. Valverdel, P. Cuevas, A. Romero, G. Giménez-Gallego, *J. Biol. Chem.* **2003**, *278*, 21774–21781; b) J. Angulo, P. Cuevas, B. Cuevas, M. El Youssef, A. Fernández, E. Martínez-Salamanca, R. González-Corrochano, G. Giménez-Gallego, *J. Transl. Med.* **2015**, *13*, 48; c) Y. Li, W. Wang, Y. Zhang, X. Wang, X. Gao, Z. Yuan, Y. Li, *Biomater. Sci.* **2019**, *7*, 1584–1597.
- [22] R. Schimidt, E. Afshari, *J. Phys. Chem.* **1990**, *94*, 4377–4378.
- [23] T. Dumsla, B. Yang, A. Maghsoumi, G. Velpula, K. S. Mali, C. Castiglioni, S. D. Feyter, M. Tommasini, A. Narita, X. Feng, K. Müllen, *J. Am. Chem. Soc.* **2016**, *138*, 4726–4729.
- [24] Q. D. Liu, R. Wang, S. Wang, *Dalton Trans.* **2004**, *14*, 2073–2079.

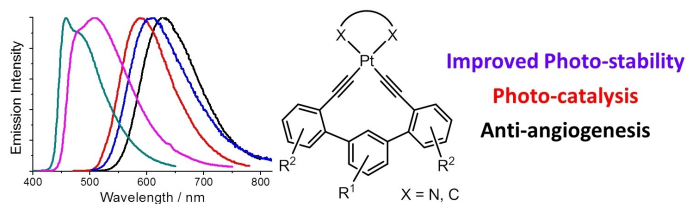
Manuscript received: July 5, 2021

Revised manuscript received: August 7, 2021

Accepted manuscript online: August 9, 2021

Version of record online: ■■■, ■■■■

FULL PAPER



A series of platinum(II) complexes supported by terphenyl diacetylide as well as diimine or bis-*N*-heterocyclic carbene (NHC) ligands have been prepared. The diacetylide ligands adopt a *cis* coordination mode

featuring non-planar terphenyl moieties. Furthermore, the electrochemical, photophysical and photochemical properties of these platinum (II) complexes have been investigated.

Z. Luo, Dr. Y. Liu, Dr. K.-C. Tong,
Dr. X.-Y. Chang, Dr. W.-P. To*,
Prof. Dr. C.-M. Che*

1 – 16

**Luminescent Platinum(II)
Complexes with Bidentate Diacetylide Ligands: Structures, Photophysical Properties and Application Studies**

